Nature of the Low Field Transition in the Mixed State of High Temperature Superconductors

Seungoh Ryu[+] and David Stroud
Department of Physics, Ohio State University, Columbus, OH 43210
(February 1, 2008)

We have numerically studied the statics and dynamics of a model three-dimensional vortex lattice at low magnetic fields. For the statics we use a frustrated $3D$ XY model on a stacked triangular lattice. We model the dynamics as a coupled network of overdamped resistively-shunted Josephson junctions with Langevin noise. At low fields, there is a weakly first-order phase transition, at which the vortex lattice melts into a line liquid. Phase coherence parallel to the field persists until a sharp crossover, conceivably a phase transition, near $T_\ell > T_m$ which develops at the same temperature as an *infinite* vortex tangle. The calculated flux flow resistivity in various geometries near $T = T_\ell$ closely resembles experiment. The local density of field induced vortices increases sharply near T_ℓ, corresponding to the experimentally observed magnetization jump. We discuss the nature of a possible transition or crossover at T_ℓ(B) which is distinct from flux lattice melting.

I. INTRODUCTION

Ever since their discovery, the behavior of high-T_c materials in a magnetic field has seemed mysterious [1]. Unlike the conventional low-T_c type-II materials, high-T_c superconductors (HTSC's) show a broad region in the magnetic-field/temperature (H-T) plane where the Abrikosov lattice has apparently melted into a *liquid* state [2].

Considerable recent evidence now suggests that flux lattice (FL) melting is a *first-order* phase transition. On the experimental side, a local magnetization jump has been measured by network of Hall microprobes [3] on $Bi_2SrCa_2Cu_2O_8$ and has been associated with the melting transition. The transition thus observed seems to lie quite near the melting curve as determined from low angle neutron diffraction [4] and μSR experiments [5]. More recently, Schilling *et al* [6,7] have directly observed the latent heat of the transition in $YBa_2Cu_3O_{7-\delta}$ along a line $T_m(H)$ in the $H-T$ phase diagram which agrees well with mechanical and transport measurements [8–10]. Numerical evidence for a first order melting transition has been obtained from simulations based on a frustrated XY model [11,12], and from a lowest Landau level model which is expected to be most accurate at high magnetic field [13]. First order melting has also been observed numerically in a system of unbreakable flux lines described by a Lawrence-Doniach model [14]. All these simulations are based on a large density of flux lines ($\sim \mathcal{O}(1-10)$tesla).

An anomalous feature of the local Hall probe measurements is that the apparent first order transition line seems to terminate at a critical point above which the latent heat vanishes [3]. Since on symmetry grounds a first order "melting" line cannot terminate in a critical point [15], this critical point may suggest that the first order melting line is instead intersecting another phase transition line related to the disorder. A related issue is the entropy released per vortex per layer across the transition line. This entropy increases very rapidly as the field decreases. Such behavior is difficult to accounted for within a model based only on the field induced vortices.

In the presence of disorder, the lattice becomes unstable at high fields against proliferation of quenched-in topological defects [16,17], possibly through a first order phase transition across a horizontal (constant H) line in the H-T plane. This line then may meet the temperature-driven melting line, causing it to terminate. Somewhere along this line, the melting transition may be converted into the universality class of the continuous vortex glass transition [18], characterized by divergent correlation lengths and times.

Another unresolved issue regarding the phase diagram is the possibility of reentrant melting at low fields. Reentrant flux lattice melting is expected because of screening of the widely-separated vortex lines at low fields [2,19]. It has been recently reported in single-crystal $NbSe_2$ sample [20], based on tracking of the so-called "peak effect" [21,22]. Such reentrance behavior has been observed only at the limited field range by Ling *et al* [23]. On the other hand, the melting curve tracked by the micro-Hall probe [3] seems to monotonically approach the zero-field superconducting transition at $T_c(H=0)$ even for fields as low as a few Gauss.

FL melting can also be probed by transport measurement. But since such measurements are non-equilibrium, they offer only an indirect means of studying *equilibrium* FL melting. In real materials with disorder, the interpretation of transport measurement is further complicated by the many competing energy scales. In single-crystal $YBa_2Cu_3O_{7-\delta}$,

the in-plane resistivity exhibits a discontinuous jump and hysteresis which have been identified with a first-order melting transition [8]. Nonetheless, the peak effect in the critical current occurs at slightly lower temperatures than the resistivity jump, leading some workers to postulate that there is a "premelting" phenomenon [21] in this material, in addition to melting. In $Bi_2SrCa_2Cu_2O_8$, simultaneous transport and local magnetization measurements [24] show that the jump in local magnetization M coincides (at high fields) with a jump in the resistivity ρ_{ab} from zero to a finite value, or (in low fields) the continuous development of a finite ρ_{ab}. In addition, at high fields, the jumps in ρ and M are accompanied by hysteresis. Together, these phenomena strongly suggest first order flux lattice melting at high fields. At low fields, the experiments are more ambiguous.

FL melting has been widely studied numerically. The possibility of *two stage* melting was first suggested by Li and Teitel [25,26] for a model with infinite penetration depth λ, and later for a system with finite λ [27,28]. The calculations of Li and Teitel are based on the so-called frustrated XY model with fairly low flux per plaquette of $f = 1/25$ (in units of the flux quantum $\Phi_0 = hc/2e$) on a simple cubic lattice. They find that the three-dimensional flux line lattice (3D FLL) melts first into a "line liquid" characterized by disentangled flux lines, which become entangled at a second, higher-T phase transition. Current-voltage (IV) measurements in the so-called "flux transformer" geometry [29–32] provide some support for this picture. Specifically, they suggest that FL melting is signaled by the onset of finite in-plane resistance, while in an applied current, phase coherence is lost in the c direction only at a distinctly higher temperature. On the other hand, simulations of dense (f=1/6) flux lines on a stacked triangular grid favor a single transition [11,12]. Dynamical calculations [33] on a triangular lattice at $f = 1/6$ suggest that if there are two separate transitions, they arise from pins, either intrinsic to the discrete cubic grid, or put in by hand. Yet more recent studies based on a London vortex loop model on a simple cubic lattice show that superconducting order disappears apparently in two steps, the sequence of which depends on the lattice anisotropy [34], although it is argued to be a finite size effect by the same authors [35].

In this paper, we attempt to resolve some of these issues by considering the frustrated XY model over a *wide range of flux densities*, using both static and dynamic simulations but with no quenched disorder. By examining this model on a stacked triangular lattice, we minimize the unphysical periodic pinning due to the lattice. By working at relatively low densities, we focus on the regime, now being probed experimentally, where the XY phase fluctuations (vortex loops) are as important as those of *field induced* vortex lines [36]. Our main conclusion is that there are, in fact signatures of two separate transitions at low fields, which are not artifacts of pinning by the discrete grid. The transition at lower temperature is unambiguously associated with vortex lattice melting. The second transition may be a sharp crossover rather than a true phase transition. Nevertheless, it is responsible for several experimental features (such as sharp increases in local magnetization and in resistance) which are often identified as evidence for a first order melting transition.

The remainder of this paper is organized as follows. In Section II, we describe our model and its numerical solution. The following sections present our numerical results, which are followed by a discussion and then summarized in a concluding section.

II. MODEL

A. Hamiltonian and Thermodynamics

We study the standard frustrated XY model described by the Hamiltonian

$$\mathcal{H} = -J \sum_{\langle ij \rangle} \cos(\theta_i - \theta_j - A_{ij}), \tag{1}$$

where $A_{ij} = \frac{2\pi}{\Phi_0} \int_i^j \mathbf{A} \cdot \mathbf{dl}$, $\mathbf{A}$ is the vector potential associated with a uniform magnetic field $\mathbf{B} = B\hat{z}$ applied parallel to $\hat{z}$, $\Phi_0 = hc/2e$ is the flux quantum, θ_i is the phase of the order parameter on site i, and the sum runs over nearest neighbor pairs. We use a stacked triangular grid with $\mathbf{B} \| z$, the direction perpendicular to the triangular network, with periodic boundary conditions (PBC) in all directions except where stated otherwise.

To allow a wider range of frustrations compatible with the boundary conditions, we use a variant of the Landau gauge [37]. Note that there are four bonds per grain: three in the xy-plane and one along $\hat{z}$. We label these by their unit vectors $\hat{\alpha} = \hat{x}, \hat{y_1}, \hat{y_2}, \hat{z}$ where $\hat{y_1} = (1/2)\hat{x} + (\sqrt{3}/2)\hat{y}$ and $\hat{y_2} = -(\sqrt{3}/2)\hat{x} + (1/2)\hat{y}$. The phase factors A_{ij} connecting a grain located at (x,y,z) to its four nearest neighbors are given by 0 along $\hat{x}$ or $\hat{z}$, $2\pi f(2x+1/2)$ along $\hat{y_1}$, and $2\pi f(2x-1/2)$ along $\hat{y_2}$. There are exceptions to this form for grains lying on the boundaries: All grains lying on the $x = \mathrm{L}_x$ boundary plane have $A_{ij} = -2\pi \cdot 2\mathrm{L}_x y$ for bonds in the x direction. Bonds at $x = \mathrm{L}_x$ boundary such that $\mathrm{mod}(j, 2) = 1$ have $A_{ij} = 2\pi f[2x + 1/2 - 2\mathrm{L}_x(y+1)]$ in the y_1 direction. For bonds on the $x = 0$ boundary with

$\mathrm{mod}(j,2)=0$, $A_{ij}=2\pi f[2x-1/2+2\mathrm{L}_x(y+1)]$ for bonds in the y_2 direction. In contrast to the usual Landau gauge (which is compatible with frustrations only in integer multiples of $1/(2N_x)$), this generalized gauge is compatible with any f which is an integer multiple of $1/(2N_xN_y)$ under periodic boundary conditions.

We have considered networks of sizes $\mathcal{N}=N_x\times N_y\times N_z$. For $f=1/24$, we have studied $N_z=12,24,48$ and $N_x=N_y=24$, and for other values of f (1/2592, 1/1648, 1/81, and 1/6) we have considered $N_x=N_y=N_z=18$. In two dimensions, the vortices lie on the vertices of a honeycomb grid of unit length of $(1/\sqrt{3})a_B$ which is dual to the triangular grid of unit length a_B. Assuming that vortices form perfect triangular lattice on this grid, and equating the area per vortex to $(\sqrt{3}/4)a_B^2/f$, we obtain the following necessary condition for a triangular vortex lattice to form without *geometric frustration* of the FL:$2/f=(n_1^2/3+n_2^2/4)$ with integers n_1,n_2. The values of $1/f$ satisfying this condition are then $2,6,8,14,18,24,32,38,42\ldots,648,\ldots$. For $f=1/162$, two distinct pairs [(n_1,n_2) = (0,36), and (27,18)] satisfy the condition. $f=1/648$ has the lowest possible nominal vortex density of one per 18×18 system compatible with our chosen gauge, and allows either of the pairs (n_1,n_2) = (0,72) and (54,36). $f=1/2592(=1/4\times\frac{1}{2\times18\times18})$, represents less than a single vortex line, and the system is *gauge-frustrated*.

In practice, for $f\leq1/81$, there are too few field-induced flux lines to study FL melting. Nonetheless, the dilute regime is still of interest, since in these cases, the flux lines behave independently and the thermodynamics is dominated by the zero-field phase degrees of freedom [36]. Except for f = 1/2592, we study only gauge-unfrustrated values allowing only an integer number of vortices in the simulation box.

We calculate the thermodynamics using a standard Monte Carlo (MC) algorithm, with up to 10^6 MC steps at each temperature T. To ensure equilibration in the ground state for all values of f, we performed simulated annealing runs for the two-dimensional (2D) version at each f with the same lateral dimensions. We then form the ground state of the 3D system by stacking the 2D ground states thus found uniformly along the $z-$direction. This enables us to find the ground state configuration of a perfect triangular lattice for low values of $1/24\leq f\leq1/18$ within a reasonable time. Starting from these 3D ground states, we warm up the system in steps of $\triangle T/J=0.05$ or 0.1, allowing at least $4-5\times10^4$ Monte Carlo sweeps for each T. The final configuration for each T is then saved to be used as a starting configuration in some of the longer calculations as well in the dynamic simulations.

From these calculations, we extract a range of thermodynamic quantities. One of these is the specific heat $C_V=(\langle H^2\rangle-\langle H\rangle^2)/(k_BT)$ at temperature T. We also calculate the local vorticity vector field $n_\alpha(p)$ defined for each Cartesian direction α and each point p of the stacked honeycomb dual lattice. At each instant during the simulation, $n_\alpha(p)$ is determined from

$$\sum_p^\alpha \mathrm{mod}[\phi_\mathrm{i}-\phi_\mathrm{j}-\mathrm{A_{ij}},2\pi]=2\pi[\mathrm{n}_\alpha(\mathrm{p})-\mathrm{f_p}]. \tag{2}$$

Here the summation runs along the bonds belonging to the plaquette labeled p,α (a triangle in the xy plane, a square in planes parallel to the z axis); and $f_p\equiv\sum_p^\alpha A_{ij}/(2\pi)$. From n_α, one can also compute the *structure factor*, $S_{\alpha\beta}(\mathbf{k})=\langle n_\alpha(\mathbf{k})n_\beta(-\mathbf{k})\rangle$, where $n_\alpha(\mathbf{k})$ is the Fourier transform of the local vorticity vector $\mathrm{n}_\alpha(\mathbf{r})$. We also calculate the principal components γ_{xx} and γ_{zz} of the helicity modulus tensor [38], in the directions perpendicular and parallel to the applied field. To within a constant factor, γ represents the phase rigidity or the superfluid density tensor of the system; its derivation in terms of equilibrium thermodynamic averages has been given elsewhere [39].

B. Dynamics

To treat the dynamics, we model each link between grains as an overdamped resistively shunted Josephson junction (RSJ) with critical current $I_c=2eJ/\hbar$, shunt resistance R, and Langevin white noise to simulate temperature effects. The effective IV characteristics are then obtained by numerically integrating the coupled RSJ equations, as described elsewhere [40], using a time constant typically of $0.1t_0$ and obtaining voltages by averaging over an interval of $\sim600t_0-2000t_0$. Since direct solution of these equations would involve inverting and storing an $\mathcal{N}\times\mathcal{N}$ matrix, where $\mathcal{N}$ is the total number of grains$\sim\mathcal{O}(5000)$, we instead solve them iteratively [41], incurring a speed penalty of a factor of $\ln\mathcal{N}$. We verified that our solutions converge by comparing them with those from direct inversion for time steps of $0.01,0.04$ and 0.1 on an $8\times8\times8$ system.

The most obvious approach to the dynamics of this model would be to use free boundary conditions, injecting current into one face of the lattice and extracting it from the opposite, with periodic transverse boundary conditions [42]. But this has the following disadvantage. Once the flux lattice is depinned from its underlying periodic pinning potential, it will drift along *as a whole* under the influence of the Lorentz force provided by the driving current. Since this occurs equally in the solid and the liquid state, such a geometry may not distinguish clearly between flux lattice and flux liquid (in the absence of spatially inhomogeneous pinning centers). This problem may be even more

conspicuous in our stacked triangular geometry, since the critical current I_{dp} for depinning a single vortex pancake from the underlying triangular grid at zero temperature (T = 0) is smaller ($I_{dp} \approx 0.037 I_c$) than in a square grid ($I_{dp} \approx 0.1 I_c$) [43].

We therefore adopt a different geometry for injecting and extracting current, as shown in Fig. 1. Fig. 1 (a) corresponds to injecting current I/I_c into each grain in the yz plane at x = 0, and extracting it from each grain at $x = N_x/2$ (with periodic boundary conditions in all three directions). In this geometry, the Lorentz forces acting on the vortices in the two halves of the volume are oppositely directed, as indicated by the arrows. Thus, in this geometry, we are effectively probing the *shear modulus* μ of the vortex lattice, on a length scale $L_x/2$. Similar geometries have been previously discussed in the context of possible experiments [44,45]. In Fig. 1 (b), we show a geometry which is designed to probe the *c-axis resistivity*, ρ_c. In this case, we inject a current I into each grain on the xy plane at $z = 0$ and extract it from each grain at $z = N_z/2$. There is on average no Lorentz force on the vortex lines.

III. ZERO-FIELD XY MODEL: F = 0

A. Thermodynamics

The 3D unfrustrated XY model on a *cubic grid* has been extensively studied [46]. Near the phase transition, the specific heat $C_V \sim |T - T_{XY}|^{-\alpha}$ with $\alpha \sim 0$ and the correlation length $\xi \sim |T - T_{XY}|^{-\nu}$ with $\nu \sim 0.66 - 0.67$. For a cubic lattice, $T_{XY} \sim 2.203J$. In a stacked triangular grid, where each grain has more nearest neighbors, the transition is shifted to a higher temperature. Numerically, we find that $T_{XY} \sim 3.04J$.

The XY phase transition is best characterized by the *helicity modulus tensor* $\gamma_{\alpha\beta}$, which measures the phase rigidity of the system [38]. In stacked triangular lattice, this tensor is diagonal with elements

$$\begin{aligned}\gamma_{\alpha\alpha} &= \frac{1}{V}\frac{\delta^2 \mathcal{F}}{\delta A^*_\alpha \delta A^*_\alpha} \\ &= \frac{J}{V}\Big\langle \sum_{ij} \cos(\Theta_{ij}) \hat{n}_{ij} \cdot \hat{n}_\alpha \Big\rangle - \frac{J}{k_B T} \times \\ &\quad \Big(\Big\langle [\sum_{ij} \sin(\Theta_{ij}) \hat{n}_{ij} \cdot \hat{n}_\alpha]^2 \Big\rangle - \Big\langle \sum_{ij} \sin(\Theta_{ij}) \hat{n}_{ij} \cdot \hat{n}_\alpha \Big\rangle^2 \Big). \end{aligned} \tag{3}$$

Here A^*_α is a fictitious uniform vector potential in the α direction, V is the volume, $\Theta_{ij} = \theta_i - \theta_j - A_{ij}$ is the gauge-invariant phase difference, $\hat{n}_{ij}$ and $\hat{n}_\alpha$ are unit vectors along the ij^{th} bond and in the α direction.

It is useful to distinguish two contributions to Θ_{ij}: one due to spin waves, and one due to vortices [47]. The former is dominant when the $\sin\Theta_{ij} \approx \Theta_{ij}$, while the other is nonzero when the vorticities $n_\alpha(p) \neq 0$. Thus we write $\gamma_{\alpha\alpha} = \gamma^{SW}_{\alpha\alpha} + \gamma^{V}_{\alpha\alpha}$, where the two terms on the right hand side are respectively the spin wave and vortex contributions to $\gamma_{\alpha\alpha}$. The spin-wave degrees should predominate at low temperatures, while the vortex degrees of freedom are the dominant excitations near the phase transition [48–52]. The spin-wave contribution γ^{SW} can be estimated within a self-consistent harmonic approximation with the result [53]

$$\gamma^{SW} \sim J \exp\left[\frac{-k_B T}{2D\gamma^{SW}}\right] \tag{4}$$

where $D = 4$ for a stacked triangular lattice.

To characterize the vortex contribution, we introduce the *net global vorticity vector* by [54]

$$\begin{aligned}\mathcal{M}_\alpha &= \hat{n}_\alpha \cdot \int_\Sigma d\hat{\sigma} \theta_v \\ &= \int_{\Sigma^+} \theta_v d\sigma - \int_{\Sigma^-} \theta_v d\sigma \end{aligned} \tag{5}$$

where Σ^+ and Σ^- are the two bounding planes normal to $\hat{n}_\alpha$, with normal vectors parallel or anti-parallel to $\hat{n}_\alpha$. We assume that the singular portion of the phase variable θ_v has been selected out. $\mathcal{M}_\alpha$ is sensitive to existence of unbound vortex lines *perpendicular* to $\hat{n}_\alpha$. This is illustrated in the left panel of Fig. 2 for the case of a single infinite vortex line piercing the sample normal to the α direction. In this case, the phase integrals on the planes Σ^+ and Σ^- give nearly equal but opposite values. Thus $\mathcal{M}_\alpha$ has large fluctuations, leading to a reduction in the value of $\gamma_{\alpha\alpha}$ (see

below). Closed vortex loops, such as shown in the right panel, give a zero contribution to $\mathcal{M}_\alpha$. In general, for $f = 0$, the thermal average $\left\langle \mathcal{M}_\alpha \right\rangle \sim 0$. For an applied field $\parallel \hat{z}$, $\left\langle \mathcal{M}_\alpha \right\rangle \sim 0$ for $\alpha = x$ or y. It can be shown that $\gamma_{\alpha\alpha}$ and $\mathcal{M}_\alpha$ are related by

$$\gamma_{\alpha\alpha} \sim \gamma_{\alpha\alpha}^{SW} - \frac{1}{V}\frac{J^2}{k_B T}\Big\{\left\langle \mathcal{M}_\alpha^2 \right\rangle - \left\langle \mathcal{M}_\alpha \right\rangle^2\Big\}. \tag{6}$$

Thus, the vortices make a negative contribution to $\gamma_{\alpha\alpha}$ arising from fluctuations in $\mathcal{M}$. They may be said to predominate over the spin waves when their fractional contribution to the helicity modulus is of order unity, that is

$$\frac{J}{k_B T}\Big\{\left\langle \mathcal{M}_\alpha^2 \right\rangle - \left\langle \mathcal{M}_\alpha \right\rangle^2\Big\}/\mathcal{N} \sim \mathcal{O}(1) \tag{7}$$

where $\mathcal{N}$ is total number of grains.

In Fig. 3, we show the calculated γ_{zz}, as well as the value γ_{zz}^{SW} determined from the self-consistent harmonic approximation (SCHA), eq. (4). The other principal components of γ behave similarly. γ_{zz} and γ_{zz}^{SW} begin to differ for temperatures as low as $T \sim 0.3 T_{XY}$, where vortex loops start to be excited. The SCHA predicts a discontinuous jump in γ_{SW} from a value of about 0.37 at T_{XY} to zero. This jump is an artifact of the approximation, which neglects the periodicity of the Hamiltonian in the angle variables and the vortex fluctuations. The inset shows a finite size scaling analysis to locate T_{XY}. The helicity modulus $\gamma \sim |T - T_{XY}|^v$ with $v = (d-2)\nu$. Therefore, the scaled quantity γL for an $L \times L \times L$ system should cross a single point at T_{XY}. Based on this criterion, our numerical results give $T_{XY} = 3.04J \pm 0.02$. We also observe that $\gamma(T)$ approaches zero with $v \sim 2/3$ for $0.02 < |T_{XY} - T|/T_{XY} < 0.1$ and deviates from this outside the range.

Eq. (6) is equivalent to that derived in Fourier space by Chen and Teitel [28] for $\lambda \to \infty$:

$$\gamma_{zz}(q\hat{x}) = J\Big[1 - \frac{4\pi^2 J}{VT}\frac{< n_y(q\hat{x}) n_y(-q\hat{x}) >}{q^2}\Big]. \tag{8}$$

if we take $q \to \pi/\mathrm{L}_x$.

An alternative form based on the vortex loop scaling picture has been obtained by Williams [55] in the limit $\lambda \to \infty$ where $\gamma_{\alpha\alpha}$ is given in terms of vortex loop diameter distribution. To check the importance of large loops, we show in Fig. 4, our calculated size distribution of *connected vortex loops* near T_{XY}. Two vortex segments are considered *connected* if they cross within a single unit cell. Such crossings become very extensive at T_{XY}, suggesting that the energy barrier for vortex line intersections vanishes near T_{XY} For $T < T_{XY}$, the maximum vortex loop size is finite, while for $T \geq T_{XY}$, there start to occur vortex lines spanning the entire simulation cell. Thus T_{XY} somewhat resembles a bond-percolation transition, although T_{XY} does not correspond to the percolation threshold, but to a point where connected cluster first forms a $D-1$ dimensional manifold if the system is in dimension D. Because such infinite clusters occur, it appears that the behavior seen in Fig. 4 is not a consequence of the finite simulation cell, but persists in the thermodynamic limit. A similar picture, but with no long-range interactions among the vortex segments (the so-called polymer limit), has been discussed by Akao [56] and by Kultanov *et al* [57].

B. Dissipation near T_{XY}

We have also calculated the dissipation near $T_{XY}(f = 0)$, using the periodic current injection geometry of Fig. 1, In this case, since there are no field-induced vortex lines, the calculated dissipation can be unambiguously related to the resistivity. Our results are shown in Fig. 5 for several values of the bias current density. [More details of the method are described in section VI D.] To calculate the differential resistance, dV/dI, we carried out two separate runs at $I/I_c = 0.083$ and 0.043, to obtain $dV/dI = V(0.083) - V(0.043)/0.04$. Fig. 5 shows this result as well as $R \equiv V(0.083)/I$ in the inset. These bias currents are low enough to show sharp features at $T_{XY}(f = 0)$ while not significantly disrupting that transition. At higher current densities (not shown), there are numerous current-induced vortex loops. These increasingly round out the sharp jump at $\mathrm{T}_{XY}(f = 0)$ shown in the Figure, which eventually washes away entirely.

Fig. 6 shows the average number of vortex segments per plaquette as calculated both by Monte Carlo simulations (with no driving current) and by coupled RSJ dynamics (with a finite bias current). Evidently, just at the XY transition, the system becomes filled with thermally generated vortex segments, *one per grain, or elemental cell.* Below $T_{XY}(f = 0)$, while there may exist vortex loops of arbitrary size, the number of these, $\mathcal{P}(l)$, falls off exponentially for large clusters (cf. Fig. 4). By contrast, for $T \geq T_{XY}$, $\mathcal{P}(l)$ diminishes algebraically with l. This subtle change in

$\mathcal{P}(l)$ implies that the average size of the connected vortex tangle remains finite for $T < T_{XY}$, but diverges above it [48]. We find that there are numerous *finite* vortex loops at temperatures as low as $0.5T_{XY}$. Moreover, at any given temperature, we find that a large bias current further enhances both their number and their size.

A simple argument suggests that the dissipation below $T_{XY}(f = 0)$ may be exponentially activated. The effective energy for a vortex loop of radius r oriented normal to a uniform driving current density j is $U(r) \sim 2\pi r \cdot \mathrm{Min}[\ln(r), \ln(\lambda)] - c \cdot \pi r^2 j$, where λ is the penetration depth. Thus, there is a barrier to loop expansion with a critical radius $r_c \sim \ln\lambda/j$ and height $U_{max} \sim (\ln\lambda)^2/j$. For sufficiently small j, only those vortex loops of size $r > r_c$ will expand and contribute to dissipation. From our simulations, for $T < T_{XY}$, $\mathcal{P}(l)$ decays exponentially. Therefore, the small dissipation involving the expansion of thermally nucleated vortex rings should have an activated temperature-dependence for $T < T_{XY}$, resulting in highly nonlinear IV characteristics.

IV. DENSE LIMIT: F = 1/6

This is the largest value we studied which allows a triangular vortex lattice commensurate with the underlying triangular grid. This value yields a strong first order transition [11,12], with an entropy of melting ΔS of about 0.3 k_B per vortex pancake.

In the present MC simulation, the lattice was gradually warmed up from a perfect triangular lattice in temperature steps of $dT = 0.1J$, with 50,000 MC sweeps for each T. The insets show the in-plane density-density correlation $< n_z(\mathbf{r}_\perp, z)n_z(0,0) >$ for $T/J = 1.175$ and 1.3, slightly below and slightly above the melting temperature. At the melting temperature T_m, our MC histogram for the internal energy distribution agrees with that of [11]. We have also calculated both $\gamma_{zz}(T)$ and the Bragg intensity $S_{zz}(\mathbf{G}_1)$ at the smallest reciprocal lattice vector $\mathbf{G}_1$ for the triangular vortex lattice. The results are shown in Fig. 7. To within $\delta T/J \sim 0.025$, both quantities vanish close to $T = T_m(1/6) \sim 1.175J$, the melting temperature as determined from the double peaks in the energy histogram [11]. The apparent melting $T \approx 1.2J$, slightly higher than inferred from the energy histogram, seems to be due to a superheating effect.

The occurrence of only a single phase transition at $f = 1/6$ [11,33] is not surprising: at this field, there is one vortex pancake for every three grains, and hence, only three phase degrees of freedom per pancake. Thus, most potential vortex excitations are already exhausted by the lateral fluctuations of field-induced vortex lines in the liquid phase. This can be seen in Fig. 8, where we show two typical vortex configurations, one slightly below and the other above the melting transition. Clearly, the transverse line fluctuations quickly dominate the thermodynamics above T_m. The strong first order transition at $f = 1/6$ can be then understood by the close connection between the lateral line fluctuations and incipient vortex loops. We conclude, with an accuracy of $dT/J = 0.025$, that in the dense limit of $f = 1/6$, superconducting coherence is destroyed in all directions as soon as the lattice melts.

V. DILUTE LIMIT

By *dilute limit*, we mean the regime where the number density of thermally excited vortex line segments n_c equals or exceed the density of field-induced vortex line segments. To make this more quantitative, we first consider a perfect line lattice at $T = 0$ with a given f. The number of unit vortex line segments *per grain* will be $1/(3f)$, or $1/(15f)$ per plaquette (since there are five plaquettes per grain). Thus, for $f = 1/6$, there are 0.4 vortex segments per plaquette. In Fig. 6, we show the density n_c of *thermally excited* vortex segments at $f = 0$, including all three directions. Note that at the XY transition, $n_c \equiv 0.15$. Thus, $f = 1/6$ is clearly in the dense regime, while $f < 1/18$ is roughly in the dilute regime.

Fig. 9 shows the specific heat C_V per grain, as calculated from energy fluctuations for several values of f [1/162 (4 flux lines), 1/81, 1/24, 1/18 and 1/6 (108 lines)] in both the dilute and dense regime. At low T, all the C_V's approach $k_B/2$ per grain, as expected from the Dulong-Petit law. The overall behavior of the peaks in C_V up to $f = 1/24$ is remarkably similar to that seen in $YBa_2Cu_3O_{7-\delta}$ [58]. For $f = 0$, it is known that C_V has a weak divergence ($\propto |t|^{-\alpha}$ with $\alpha \approx 0.0$ [46]), as expected for the $3D$ XY model. At finite f, this peak is rounded as seen experimentally [58,59]. As discussed below, these broad peaks in C_V generally occur *well above* the melting transition in this field range. Note that our results for the dense ($f = 1/6$) case differ qualitatively from all those at lower f. The sharp peak for $f = 1/6$ is actually a delta-function singularity, consistent with the finite heat of fusion of a first-order transition known to occur at this density [11].

Fig. 10 shows that the height of the peak for $f \leq 1/18$ roughly follows a logarithmic dependence on the magnetic length L_B defined as $L_B = 1/\sqrt{f}$, the average vortex spacing. Furthermore, as we show in Fig. 11, the position of the peak at a finite f shifts from $T_{XY}(f = 0)$ by an amount $\delta T_c(L_B)$ which closely follows the law $\sim L_B^{-3/2}$. As we will

show in more detail for $f = 1/24$ below the phase rigidity along the applied field, as measured by γ_{zz}, vanishes for all f near the broad maximum in specific heat. At the temperatures [which we denote $T_\ell(f)$] where $\gamma_{zz}(f)$ vanishes, we observe that the average number of thermally generated vortex segments *per grain* normal to the $\hat{z}$ direction closely follows the law $n^c_{xy}(T_\ell) \sim 0.1 \cdot L_B^{0.6\pm0.1}$. All this behavior is discussed in more detail below.

VI. F=1/24

A. Statics: Melting and γ_{zz}

In the dilute regime, such as $f \leq 1/24$, there are numerous phase degrees of freedom per field-induced vortex pancake. Thus, a double transition, if there is one, might be more plausible here than at $f = 1/6$, one transition being the melting of the field induced flux lattice, the other connected to the XY-degrees of freedom [36].

To check this possibility, we have studied $f = 1/24$ (a field which allows for a commensurate triangular flux lattice of 48 lines) on a stacked triangular grid of $24 \times 24 \times 24$ grains. We first did an extensive simulated annealing run on a single layer, verifying that the vortices freeze into a perfect triangular lattice. We then stacked 24 such layers to form a three dimensional ground state. Next, the lattice was gradually warmed up in intervals of $dT/J = 0.1$ or 0.05, typically with 50,000 MC steps for each temperature. For several T close to a transition, we ran up to 10^6 MC steps to ensure equilibration. The resulting Bragg intensity $S(\mathbf{G}_1)$ and helicity modulus component $\gamma_{zz}(T)$ are plotted in Fig. 12. [The transverse components $\gamma_{xx}(T)$ and $\gamma_{yy}(T)$ fluctuate around zero for most $T > 0$, as expected for a very weakly pinned vortex lattice which is free to slide in the *ab* plane.]

The results do indeed suggest the possibility of *two* phase transitions. The first - the melting of the vortex lattice - occurs near $T = 1.5J \equiv T_m$, where the Bragg intensity drops sharply. At higher temperatures, there is a broad dip in the normalized Bragg intensity which reaches a plateau at around $T/J \sim 2.1$. The possible upper transition, near $T = 2.0J \equiv T_\ell$, is the point where $\gamma_{zz}(T)$ vanishes. Essentially the same behavior, but with an even wider temperature separation, has previously been observed on a cubic grid by Li and Teitel [25].

We have carried out several checks to see if the separation of these two transitions is an artifact due to a finite-size effect. First, as shown in the inset, we monitored the dependence of γ_{zz} on accumulation time τ up to 10^6 MC steps. More precisely, we define $\left\langle A \right\rangle_\tau \equiv \frac{1}{\tau}\int_0^\tau A(t)dt$ and use this in calculating the averages which define γ_{zz} in eq. (3). The $< \gamma_{zz}(T) >_\tau$ thus defined generally evolves approximately logarithmically in τ [60] until it reaches its apparent equilibrium value. For temperatures $T_m < T < T_\ell$, the system tends very slowly towards an apparently *finite* limiting value. We have also checked the size dependence up to $24 \times 24 \times 48$, verifying that the $24 \times 24 \times 24$ behavior represents the asymptotic limit. Li and Teitel have carried out similar checks up to 200 layers in the cubic model [26]. Nonetheless, γ_{zz} has some size- dependence to a degree dependent strongly on anisotropy of the system.

If the ratio J_z/J_{xy} is increased to 4.0 (where J_z and J_{xy} are the couplings perpendicular and parallel to the triangular plane), the separation $(T_\ell - T_m)/J_{xy}$ between the melting transition and the upper possible transition actually grows for a given size. For these values, the smallest-$\mathbf{Q}$ Bragg peak vanishes at $T_m \sim 2.9J_{xy}$, while γ_{zz} vanishes at $T_\ell \sim 4.0J_{xy}$. On the other hand, for weakly coupled layers with $J_z/J_{xy} = 0.1$, the two transitions merge to within less than $0.1J_{xy}$, as in the the *isotropic* dense $f = 1/6$ case. In this weakly coupled case, $T_m \sim 0.6J_{xy}$.

These observations suggest that phase coherence at finite f in a disorder-free system may possibly be destroyed in two steps. First, coherence transverse to the average field direction is lost through melting of the lattice. But longitudinal coherence persists until it is destroyed, along with line-like correlations of the individual vortex segments, at a slightly higher temperature T_ℓ. This is most apparent for the *isotropic* system only when $f \leq 1/18$.

B. Vortex Analysis of Possible Transition at T_ℓ

There are several ways to look at general phase correlation function $< \Theta(\rho, z)\Theta(\mathbf{0}, 0) >$ where Θ is the gauge-invariant local phase [93] of the superconducting order parameter. To probe the longitudinal phase coherence, we only consider $c(0; z) \equiv \frac{1}{A}\int d^2\rho < \exp[i(\Theta(\rho, z) - \Theta(\rho, 0))] >$, where A is the sample area - that is, the correlation function in the $\hat{z}$ direction. Glazman and Koshelev have pointed out that phonon-like fluctuations in the vortex lattice lead to a power law decay of $c(0; z)$ [93] (not explicitly shown in the Figure 13). We observe that this holds true for $T < T_m$. For higher temperatures, this dependence changes to an exponential decay $c(0, z) \propto \exp(-z/\xi_{0z})$. The correlation length $\xi_{0z} \sim [\log(\frac{T^2}{T_0^2}\frac{\log(T/T_0)}{2\pi^2})]^{-1}$ where T_0 is the temperature scale such that $< [\Theta(0, z) - \Theta(0, z + 1)]^2 > \sim 1$. This behavior is shown for $T/T_m = 1.1$ in Fig. 13 for systems of several thicknesses. To ensure equilibration, we ran 86000 MC sweeps before accumulating data over the following 30000 MC sweeps. To check the effect of boundary conditions,

we used both open boundary (OBC) and periodic boundary conditions (PBC) along $\hat{z}$; periodic boundary condition was used in the xy plane for both cases. In all cases, we observe a robust exponential dependence over a limited range $1 < dz < \xi_x$ where deviation sets in at $dz \sim \xi_x \sim 12$ for $T/T_m = 1.1$, for example. In this temperature range, we do not find significant dependence of c(0, z) on either system size or boundary conditions. For a given temperature above T_m, we can use this robust temperature regime to extract the phase correlation length ξ_{0z} from our numerical simulation.

The result is shown in Fig. 14. For all $T > T_m$, and for separations less than $\xi_x(T)$, we observe that $c(0, z) \sim \exp[-z/\xi_{z0}]$. ξ_{z0} gradually decreases with increasing temperature approximately as $(T - T_m)^{-1}$, becoming equal to the unit layer spacing near $T/J = 3.0 \sim T_{XY}(0)$ as shown in the inset. We also observe(not shown in the Figure) that $\int d\rho c(\rho, z)$ has far milder dependence on z. The exponential decay in $c(0, z)$ is accounted for by random walk-like excursions of the vortex lines and the presence of dislocation or disclination loops in this temperature regime. Note that spinwave excitations in the vortex lattice usually lead to an algebraic decay of $c(0, z)$. Note that given a *static* deformed vortex line configuration, we may still find a coordinate transformation $\{x, y, z\} \rightarrow \{x', y', z\}$ into a curved space in which the vortex line is straight. In that coordinate system, we will have a long range phase coherence along the straight line in the $\hat{z}$ direction. Therefore, the apparent exponential decay of $c(0, z)$ is not an equivocal indicator for the destruction of phase coherence along $\hat{z}$, but gives information about the deformation of vortex lines from the straight configuration.

In the large-distance tail of $c(0; z)$, where $z > \mathrm{L}_z/2$, $c(0, z)$ does depend on the boundary conditions and system size, having an upturn for the periodic boundary condition as expected. Moreover, $\xi_{z0}(T)$ rapidly falls as T decreases toward T_{XY} from above, leaving a large interval $\xi_x(T) < dz \ll \mathrm{L}_z/2$ in which the behavior deviates from simple exponential decay and is independent of the boundary condition used. We also observe that the deviations have relatively poorer statistics due to slow kinetics. It is likely to originate from vortex entanglement and cutting/reconnection, which develop on length scales larger than ξ_{z0}. Each of these rare and slow vortex crossings produces a drastic and long-lasting impact on the local phase correlations. The rarity of these events is due to the sizable barrier for vortex cutting and to the subdiffusive nature of vortex lines motion. Because of this rarity, a rapid thermal cycling across this sluggish region may lead to hysteresis.

We now look more closely into the vortex configurations near T_ℓ for $f = 1/24$. Fig. 15 shows the density-density correlation function $n_{2,z}(\mathbf{r}_\perp, \mathrm{L}_z/2) = < n_z(\mathbf{r}_\perp, \mathrm{L}_z/2) n_z(0, 0) >$ describing the $\hat{z}$-component of local vorticity at separations equal to half the total thickness L_z (=24). The most prominent feature in $n_{2,z}$ is the disappearance of triangular correlations in the xy plane at melting ($T_m \sim 1.5J$). This behavior is consistent with the disappearance of the Bragg spots in Fig. 12. Note, however, that the central spot, corresponding to the self-correlation between the two ends of the same line, persists well above melting until it vanishes near $T/J = 2.0$, close to T_ℓ. This is consistent with the fact that line-like correlations are maintained over at least 12 layers up to $T/J = 2.0$ as we already noted in Fig. 14.

In a sample of truly macroscopic thickness, the lines in the liquid phase should carry out random-walk-like excursions, leading to loss of top-to-bottom vortex density correlations over a finite correlation length denoted $\xi_{vz}(T)$, which may be of the same order of magnitude as ξ_{0z} defined above. A finite $\xi_{vz}(T)$ means that the underlying lines are *flexible*, not that they break up into 2D vortices. This breakup becomes relevant only for $T > T_\ell$. The objects which break apart into 2D objects above the melting transition are not the lines themselves, but the *topological defects of the lattice*, such as disclinations, which tend to appear as *well-aligned* line defects near T_m [14,61]. Topological defects look well aligned only when $|\mathbf{r}_i(z) - \mathbf{r}_i(z + 1)|/a_B \ll 1$ where $\mathbf{r}_i(z)$ is the position of the segment of vortex line i in the z-th layer. Note that the relevant minimum length scale for alignment of defect lines is the mean vortex spacing, a_B. The destruction of the *lattice order* along the field, which may be detected by vanishing Bragg peak in neutron diffraction, is related to proliferation and unbinding of these defects. On the other hand, the destruction of phase coherence along $\mathbf{B}$, as we discuss in more detail later, is related to the presence of fluctuations in the transverse vorticity. As the vortex density decreases, it is not *a priori* obvious if the energy scales for these different types of defects should remain the same.

Thus the line-liquid regime, if it is really a distinct thermodynamic phase, may possibly be described as a neutral gas of topological defects (disclinations of both signs) within the triangular lattice in each plane, which are correlated over a finite length in the $\hat{z}$ direction. Above melting, one expects unbound disclinations to proliferate. Hence, the long-range structural correlations of the vortex lattice are lost in all directions upon melting. However, the *phase rigidity*, as measured by γ_{zz}, may persist even above melting, but scaled down by the factor of ξ_{z0}/L_z, the fraction of the volume of the sample into which the applied twist penetrates. Presumably, this continuous suppression, unless pre-empted by a first order transition (for high densities), persists until the condition $\mathrm{L}_z/\xi_{z0} \rightarrow \infty$ is met via proliferation of "unbound vortex loops" (vortex lines extending an infinite distance in the transverse direction). At this point, the phase coherence even between neighbouring planes normal to $\mathbf{B}$ will be lost.

In Fig. 16, we show snapshots of vortex configurations at T_m, T_ℓ and a temperature between T_m and T_ℓ. In this regime, by using a bond-searching algorithm, we have identified three distinct classes of vortex lines. The first consists of small vortex loops which close on themselves without crossing either of the two opposite bounding surfaces. The

second class contains all isolated lines beginning at the bottom xy plane and ending at the top one. Most of the disentangled field-induced vortex lines fall into this group. Finally, there occur "vortex tangles". These are lines connected at a given time to one another by the crossing of two vortex segments in the same unit cell. Such tangles are formed either by collision of two flux lines or by interactions of such lines with the vortex loop excitations. This tangle is not static: the collisions which produce it are more and more frequent with increasing temperature and its overall shape will evolve with more rapidity as T increases.

The three columns of the Figure represent the fraction of the vortices belonging to each class at a given instant. On melting ($T/J = 1.5$), the fluctuating lines in our finite sample still remain largely disentangled and separated from each other. As $T \to T_\ell$, the density of loop excitations increases (left column), while the field-induced lines (central column) have stronger lateral fluctuations . Both of these effects cause more and more "connected" clusters (i. e., vortex tangles) to appear. Finally, at T_ℓ, an *infinite* tangle, connected by crossing vortex lines, forms. At this temperature, the connected tangle of vortices form a $(D-1)$ dimensional manifold of a tortuous shape, transverse to $\mathbf{B}$, and cut the original $D(=3)$- dimensional coherent XY system into halves.

Fig. 17 shows an instantaneous vortex cluster size distribution for various temperatures at $f = 1/24$. To generate this distribution, we define the *projected transverse length* of each vortex loop (or tangle) by $\ell_{xy} \equiv \oint |\hat{z} \times \mathbf{n}_v|$ for each isolated cluster composed of unit vortex segments $\mathbf{n}_v$, and accumulate a histogram, $\mathcal{P}(\ell_{xy})$. [We consider only the size distribution projected onto the xy plane because the field induced lines (which are infinite along $\hat{z}$) could mask the loops with large extent in the z direction. We also believe that these fluctuations are more relevant to the vanishing of γ_{zz}.]

In the first panel of Fig. 17, we plot $\mathcal{P}(\ell_{xy})$ for several $T \leq T_m$. Each plot has a sharp maximum cutoff and a pronounced peak, which is due to the finite average lateral fluctuations of the field-induced vortex lines. For $T_m < T < T_\ell$ (second panel), the weight of distribution is shifted towards larger ℓ_{xy}, because lines in the liquid phase undergo larger transverse fluctuations. Closed vortex loops also begin to appear in this region. As T increases, the distribution is cut off at progressively larger values, as more and more lines join the connected clusters. Finally, for $T > T_\ell$, all curves are characterized by the appearance of "infinite" clusters, with no obvious length cutoff. The distribution appears to fall off algebraically in this regime - i. e., $\mathcal{P}(\ell_{xy}) \sim \ell_{xy}^{-\mu}$ with $\mu \sim 1.0 < 2$ - suggesting $< \ell_{xy} > \to \infty$ for $T > T_\ell$.

In Fig. 18, we show the maximum value ℓ_{xy} occurring over $10,000$ MC sweeps for each temperature. The size is normalized by the linear system dimension in the xy plane (48), and also by the number of xy-planes (24). Although ℓ_{xy} grows monotonically for $T > T_m$, it seems to jump discontinuously from ~ 1 to ~ 2 between $T/J = 2.0$ and 2.1 (near T_ℓ for samples of this size). Qualitatively similar behavior occurs for the isotropic $f = 0$ XY transition near $T_{XY}(f = 0)$ [cf. Fig. 4].

C. Entanglement, Winding Number and Other Exotica

We now discuss a possible extension of the vortex loop picture of the zero field XY transition to the hypothetical T_ℓ transition or crossover for $f \leq 1/24$. Such loop excitations have received far less attention in 3D systems [49] than their 2D counterparts, possibly because they require more energy to excite and therefore matter only very close to the mean field transition. But in high-T_c materials, the short correlation lengths, high anisotropy, and high T_c broadens the vortex-loop-dominated regime [62,63], before amplitude fluctuations set in.

In a cubic sample with periodic boundary conditions, all vortex lines naturally close on themselves to form loops. These loops are of two topological types: those which can continuously shrink to a point ("trivial class") and those which cannot ("nontrivial"). The latter are said to have a nonzero "winding number," i. e., number of infinite lines in a given direction. In the 2D periodic case, the loops lies on the surface of a torus. Here, there are two distinct subclasses of non-trivial loops: one which winds around its circumference, and another which runs transverse to it. In the infinite 2D geometry, these correspond to lines infinite in either the $\hat{x}$ or the $\hat{y}$ direction. On the 3D hypertorus, there are infinite lines in any of *three* directions.

These notions play critical role in the description of dissipation via vortex motion, i. e. phase slips [64]. For current flowing in a given direction, the dissipation may occur either through the expansion of loops, or through motion of an infinite line. In either case, the dissipation arises from fluctuations in the winding number of vortex lines perpendicular to the current(c. f. Equations (6) and (7)). Note that when a finite field is applied along $\hat{z}$ direction, the hypertorus already contains many "windings" along that direction even without an applied current.

In the absence of pinning, dissipation in the plane normal to $\hat{z}$ is governed by fluctuations of the winding number in the $\hat{z}$ direction. This dissipation should not depend directly on whether or not the "windings" - that is, the vortex lines - form a lattice, but may depend on the *density* and mobility of windings.

Dissipation parallel to the field direction (c-axis resistance) depends mainly on winding number fluctuations transverse to $\hat{z}$. Clearly, the average winding in this direction vanishes, unless the field-induced lines themselves, while winding along $\hat{z}$ as required, also wind along another direction like wires around a solenoid. For this to occur, the lines would have to break a chiral symmetry, spontaneously generating a global surface current with a net magnetization normal to $\hat{z}$ - an effect which should be prohibited energetically in the ground state.

It may occur, however, if there exist entangled field induced vortex lines which collide with each other to switch connections(a process we may call "cutting and reconnection"). In Fig. 19, we show two field induced lines residing on the surface of a torus (left panel) going through such a cutting and reconnection [(panels (a)-(b)]. The right column of the figure shows an alternative view of the same process in an infinite space with open boundary conditions. Initially, both vortex lines wind only along the $\hat{z}$ axis. After the cutting and a special reconnection process in which one strand circles around the torus before meeting its other end, a net transverse winding number has been created. This "global" process is, however, energetically expensive because it involves a spatially extended excursion [panel (b)] and should occur very rarely, even in the melt.

If we introduce an "entanglement length" ℓ_c, defined as the average distance along $\hat{z}$ required for any two vortex lines to wind around each other, we expect ℓ_c to be infinite for $T < T_m$, but to become finite in the liquid phase. Because of the finite line tension and repulsive interactions between vortex line segments, such entanglement events along the flux lines are costly in energy and hence rare, in the liquid near melting. Deeper into the liquid phase, as the repulsive interaction between vortex lines is overcome by entropic forces of attraction, ℓ_c should become much shorter, leading to a much denser entanglement pattern. The now numerous local transverse fluctuations, and local cutting and reconnection events (i. e., collisions) generate fluctuations in the "global" transverse winding number and cause $\gamma_{zz} = 0$. On symmetry grounds, the average transverse vorticities $< n_x >$ and $< n_y >$ have to be zero at all temperatures. But possibly $< |n_x|^2 + |n_y|^2 >$ acquires a finite value for $T > T_\ell$, suggesting that this quantity could be used as another "order parameter" for the hypothetical phase transition at $T = T_\ell$ (with a nonzero value at *higher* temperatures).

Alternatively, we may view the upper transition in the context of a bond percolation transition. The field induced lines provide a kind of backbone network. With increasing T, vortex lines undergo more and more transverse collisions. At $T = T_\ell$, these collisions induce the entire ensemble of field-induced vortex lines to form an infinite connected $D-1$ dimensional structure transverse to the applied field, causing large fluctuations in the transverse winding number [thick gray line in panel (c)], thereby wiping out any superconducting path connecting the top and the bottom layers normal to the field.

Let the mean-square transverse displacement of field-induced vortices per layer be denoted $\ell_T^2 \equiv < |\mathbf{r}_i(z) - \mathbf{r}_i(z-1)|^2 >$. Then ℓ_c/d is defined as the number of layers along $\hat{z}$ over which a line wanders transversely by the average intervortex distance. We write this condition as $\ell_T^2 \cdot [\ell_c/d]^{2\zeta} = a_B^2$, where we introduce an unspecified "wandering" exponent ζ. In the limit of dilute (independent) lines, we expect $\zeta \approx 1/2$, corresponding to a random walk of each vortex line segment. Long-range intervortex repulsion is known to renormalize the unit step size ℓ_T from $c(T)\cdot(T/J_z)^{0.5}$ down to a smaller value with a similar form with an unspecified T dependence encoded in $c(T) < 1$ [65,66]. It is not clear how ζ is affected by intervortex repulsion, but possibly the interactions with other fluctuating lines are equivalent to the line of interest being in a random environment. For a flexible line in a 3D random environment, $\zeta \sim 0.6$ [67,68]. For $D \geq 2$, in the actual system of interacting fluctuating lines, no exact result is available for ζ, although several numerical results and conjectures give $\zeta \sim 0.2 - 0.6$ [69].

We can use these crude estimates to make a guess at the field dependence of T_ℓ, interpreted as a bond percolation transition. Along a given field-induced vortex line, the probability per unit length that a transverse connection is made to a neighbouring vortex line at any position along the $\hat{z}$-axis is $p = d/\ell_c = (\ell_T/a_B)^{1/\zeta}$. Since $\ell_T \propto (T/J_z)^0.5$ and $a_B \propto B^{-0.5}$, the percolation threshold is reached roughly when $c(T)^2 TB/J_z > [p_c]^{2\zeta}$, where p_c is an appropriate percolation threshold. This condition defines a *lower bounds* for a possible transition at $B_\ell(T)$ which approximately follows

$$B_\ell \propto \frac{[p_c]^{2\zeta}}{c(T)^2} \frac{J_z(T)}{T}. \tag{9}$$

For a dense lattice or large anisotropy (i. e., small J_z), this condition is probably satisfied immediately upon melting, as at $f = 1/6$. For dilute systems, however, the second transition is not automatically triggered by melting and may occur only deep into the liquid phase, at a temperature where the entanglement barrier is sufficiently weak to allow an infinite vortex tangle to form. Whether this percolation transition is a true phase transition or only a sharp crossover remains to be determined.

This same picture hints at how correlated pins such as columnar damage tracks [70] may increase T_ℓ. Such columnar disorder will encourage the vortex lines to stay straight along the defect track, reducing the effective unit step ℓ_T by a factor $c_p \ll c$. As a result, the wandering exponent ζ_p may also change from its thermal value ζ. Consequently, T_ℓ

will be enhanced by an overall factor of $(\frac{c}{c_p})^2(\frac{1}{p_c})^{2(\zeta-\zeta_p)}$.

In summary, the upper transition is characterized by the following set of equivalent criteria: [26,33] Disappearance of finite transverse diamagnetism; disappearance of phase rigidity along the field direction; appearance of an infinite *transverse* vortex cluster; large fluctuations in the global transverse winding number or the net vorticity $\mathcal{M}$; onset of finite c-axis phase-slip resistance in the limit of vanishing bias current in the c direction, which is equivalent to saying no superconducting path exists over macroscopic distances.

D. Dissipation for $f = 1/24$

While Bitter decoration serves as a detailed probe of spatial vortex configurations [61,71,72], it yields ambiguous information about freezing, and is restricted to very low flux densities. Cubitt *et al* obtained evidence of a melting transition in $Bi_2SrCa_2Cu_2O_8$ from low angle neutron diffraction [4]. Similar results were obtained by a μSR technique, which probes the local magnetic field distribution [5]. NMR [73] and atomic beam [74] techniques have also been used to study both the static properties and the melting of the vortex lattice. More recently, Schilling *et al* employed a differential thermometry to search for the latent heat of melting in $YBa_2Cu_3O_{7-\delta}$ and to obtain a melting curve [6,7].

Far more information has been accumulated from transport measurements, but this is much less easily interpreted in terms of vortex lattice melting. The interpretation is complicated by disorder, as well as by the fact that the measurements are nonequilibrium and usually involve nonuniform current distributions. Safar *et al* [8] measured a sharp jump in resistivity in the mixed state of $YBa_2Cu_3O_{7-\delta}$. The resistivity also showed a hysteretic behavior upon thermal cycling, indicating a first order transition. The transition line thus obtained seems to coincide with "melting curves" obtained by torque measurements [9], and more recently, by differential specific heat measurements [6]. Kwok *et al* have carefully demonstrated the effect of twin boundary pinning on the melting transition in a series of transport measurements which track the so-called "peak effect" associated with vortex lattice softening [21]. They find that the peak effect sets in at a few degrees below the melting curve determined from a sharp kink in resistivity. This sharp resistivity kink, as observed by both Safar *et al* [8] and Kwok *et al* [75], tends to become less pronounced both at very high($B > 10$ tesla) or low flux densities($B < 1$ tesla) [76].

An ideal, but impractical, transport measurement to determine the melting curve would consist of applying an infinitesimal current to induce a net Lorentz force on the lattice, which is held in place by a balancing pinning force. As soon as the lattice melts, individual lines would begin to drift, inducing "flux flow" resistance. Most real materials, however, are complicated by disorder, and even the static properties of the lattice with disorder are incompletely understood [77,78]. In the presence of disorder, varying the field density produces changes in both the effective pinning strength and the effective flux lattice anisotropy. Depending on relative strengths of all these competing effects, many complications may arise in probing thermodynamic properties using transport experiments [79–83].

A number of recent transport measurements have, nonetheless, produced rich information about flux lattice melting. Pastoriza *et al* have used a non-uniform distribution of pinning strength to probe the shear modulus directly [44], giving direct information about the lattice stability. Zeldov *et al* [3] have used local Hall probes in $Bi_2SrCa_2Cu_2O_8$ to monitor the local field density. They found a very sharp jump, again interpreted as a signature of a first order melting transition. More recently [24], Fuchs *et al* performed simultaneous measurements of the resistance and local magnetization, confirming that that the jump in local magnetic density coincides with a sharp increase in resistance (but not necessarily a discontinuous *jump*). The heat of melting *per vortex per layer* inferred from this local magnetization jump, however, shows rather peculiar features: it vanishes continuously as the field is increased, while steeply increasing as the field is lowered toward zero.

These results raise several outstanding questions: How can the seemingly first order transition line terminate apparently at a point in the H-T plane? Does the melting line monotonically approach $T_c(H = 0)$ or follow a reentrant melting curve? Another important issue is the longitudinal phase coherence probed by c-axis resistivity vs. T measurements [84,85,65], which show a striking series of broad peaks in $Bi_2SrCa_2Cu_2O_8$ single crystals. The nonlocal conductivity associated with this phase coherence can be probed in the so-called flux transformer geometry. The experimental data of Keener *et al* [31] showed that phase coherence over a finite correlation length along $\mathbf{B}$ persists above the melting transition of the vortex lattice in some region of the H-T phase diagram.

A simple and natural model for probing the dynamics of the mixed state is a network of resistively shunted Josephson junctions with Langevin noise. In this section, we present some results of simulations using this model, and to connect these to the analogous static XY results. Our calculations are carried out as follows. At any given temperature, the final snapshots from the MC simulations are used as the initial dynamical phase configurations. We use an integration time step $\triangle t = 0.1t_0$. After the current is switched on, $1000 - 5000\triangle t$ is allowed for the system to reach a steady state, following which the voltage is averaged over the next $6000 - 12000$ steps of $\triangle t$.

Fig. 20 shows the "bulk in-plane resistance" at $f = 1/24$. The measurement geometry is as shown in Fig. 1 (a); thus, these calculations probe the shear rigidity of the lattice in contrast to the usual transport experiment in which random pins play an essential and complicating role. Through the rest of this paper, we will call these calculated quantities R_{ab} and R_c, even though they differ from the resistivity measured in most transport experiments. At the highest bias current of $2.83I_c$ per grain(equivalent to $1.4I_c$ per bond), we have a smooth curve without any noticeable changes either at T_m or at T_ℓ. For lower values of driving current, sharper features emerge. There is a slope discontinuity near $T_m = 1.5J$ for both $I/I_c = 0.83$ and 0.083, but the most dramatic change occurs near $T_\ell = 2.0J$. The entangled line liquid for $T_m < T < T_\ell$ seems to have a sizable viscosity. This viscosity impedes the motion of the flux lines in the liquid, the two halves of which are driven past each other by opposing Lorentz forces. As a result, the lines move slowly, and dissipation (defined as a "resistance" R_{ab}) is small. The steady increase of R_{ab} with temperature in this region is due to screening by vortex loops which gradually lowers the viscosity. For $T > T_\ell$, this viscosity vanishes, leading to a steep increase in R_{ab} This increase at T_ℓ is enhanced by additional (and probably dominant) dissipation produced as the system goes through an XY-like transition or crossover. The large viscosity for $T_m < T < T_\ell$ is also consistent with the slow ($\ln t$) equilibration seen in the Monte Carlo measurement of γ_{zz} for $T_m < T < T_\ell$ [60]. We believe that the change in R_{ab} near T_ℓ shares the same mechanism as that seen near $T_{XY}(f = 0)$ shown in Fig. 5.

Fig. 21 shows the "c axis resistivity" R_c at f = 1/24, as calculated using the geometry of Fig. 1 (b). For comparison, we also show the calculated γ_{zz}. As the driving current is reduced, R_c seems to approach a curve which vanishes asymptotically as $T \to T_\ell^+$, coinciding with the vanishing γ_{zz}. Our numerical results thus suggest that the dramatic increase in R_c results from the T_ℓ transition rather than melting. The increase in R_c is thus correlated with massive vortex line cutting, as put forward earlier [66,65], and with an increase in the density of transverse vortex segments $< |n_{xy}| >$, the frequency of vortex line crossings, and fluctuations in the transverse net vorticity, $\delta\mathcal{M}_z^2$. This distinction between T_e and T_m may be most important for $Bi_2SrCa_2Cu_2O_8$ at low fields, and in disordered dense systems [33], where the temperatures may be most separated.

We can draw some conclusions relevant to experiment from the current dependence of both R_{ab} and R_c observed in our simulations. First, the "melting line," *as detected via a voltage criterion at constant current* in a bulk resistance measurement, should be sensitive to the driving current, even at a very low bias. Existence of pinning force is essential in getting distinct transport behaviors for the lattice and the liquid. On the other hand, the transition at T_ℓ, whether monitored by the vanishing of R_c in the limit of small current or by a jump in R_{ab} between two *finite* values, should be relatively insensitive to applied current density, since the main mechanism of dissipation(presence of transverse vorticity) in this case is switched off below T_ℓ and sets in above T_ℓ irrespective of whether we have pins or not. Indeed, just such an observation has been made by Keener *et al* [32] in describing their curves for $T_m(H)$ (melting) and $T_D(H)$ ("decoupling transition"), as obtained by flux-transformer measurements on $Bi_2SrCa_2Cu_2O_8$ single crystals. It is plausible that their $T_D(H)$ at very low fields ($B < 100$ Gauss) corresponds to T_ℓ in our model. True melting line is presumably the limiting value of the current-dependent $T_m(H, J)$ as $J \to 0$. It is not experimentally verified whether such a limiting value coincides with T_D or not.

Let us briefly comment on the experimental possibility of distinguishing between T_m and T_ℓ If we imagine a hypothetical *isotropic* high temperature superconductor, the coupling constant J in our model calculation is related to the parameters of the superconductor via $J \sim \frac{d\phi_0^2}{16\pi^3\lambda^2(0)} \times (1 - [T/T_{c0}]^4)$ (assuming the two-fluid model). Taking $T_{c0} = 92K$, $d = 10\mathring{A}$, and $\lambda(0) = 1000\mathring{A}$, we find $T_m \sim 89.7K$ and $T_\ell \sim 90.3K$ [eq. (11)]. Thus the two transitions are remarkably close even for the isotropic case. In real materials such as $YBa_2Cu_3O_{7-\delta}$ and $Bi_2SrCa_2Cu_2O_8$, the separation between the two will be further reduced by an anisotropy factor, although pinning disorder may tend to separate them. Therefore, in many cases, it will be nearly impossible to separate the two transitions experimentally.

VII. LOCAL MAGNETIZATION JUMP AND HEAT OF MELTING

A striking result of the $Bi_2SrCa_2Cu_2O_8$ micro-Hall probe measurements is the sharp jump in local magnetization (vortex density) across the phase transition [3]. At "high" fields ($\sim 200G$), the jump occurs at nearly constant T, and even for lower fields, still within $\delta T \sim 3mK$. The heat of melting per vortex per layer, $T_m \triangle S = -\frac{T_m \triangle B}{4\pi} \frac{dH_m}{dT}$, as obtained from the Clausius-Clapeyron relation, increases monotonically from 0 at $B \sim 400G$ to about $0.6k_B$ at $B \sim 55G$, beyond which the slope $\frac{dH_m}{dT}$increases very sharply (cf. Fig. 6 of [3]).

Similar jumps also seem to occur in $YBa_2Cu_3O_{7-\delta}$, as reported in recent calorimetric [6] and magnetization measurements [86,87]. The estimated latent heat of melting yields $\triangle S$ (per vortex per layer) $\sim 0.4k_B$ for $1 < B <$ 8(tesla). The data (cf. Fig. 1 of Ref. [6]) shows that the jump ΔM at $T = 85K$ ($B \sim 3.7$ tesla) for $YBa_2Cu_3O_{7-\delta}$ is spread over a field range $\delta B \sim 0.1T$, or, for a given field, over a temperature range $\delta T \sim 0.1K$. This jump decreases rather abruptly for flux densities $B \leq 1T$. The estimated entropy of melting ($\sim 0.4k_B$ per vortex pancake) is quite

close to that numerically obtained by Hetzel*et al* [11] ($\sim 0.3k_B$ per pancake), and also to the values obtained in model calculations based on the lowest Landau level and London approximations [88].

As the field decreases, the jump in M occurs over a broader temperature range (cf. Fig. 3 of [3]). The resistance jumps measured by Kwok *et al* [75], attributed to the melting transition, also become broader with decreasing field. By contrast, the height of the resistivity kink seems quite uniform over a wide range of fields. These last two observations are consistent, however, if we interpret the jump in resistance as a signal that $\gamma_{zz} \to 0$. In view of all these facts, it is plausible that, at least at relatively high fields which corresponds to $fJ_{xy}/J_z > 1/18$, the experimental jumps observed in local magnetization and resistance [3,6,75] shows the combined effects of two distinct processes, occurring within $\triangle T < 10mK$. As a corollary, the very low field measurements($fJ_{xy}/J_z < 1/18$) actually may not track the melting transition itself, but various manifestations of the predominant XY fluctuations (vortex loops) which are most conspicuous near T_ℓ..

Observation of the *reentrant* melting curve has not been reported in any high-T_c materials. In $NbSe_2$, the melting line detected by the peak effect was reported to be non-monotonic in field [20], consistent with the reentrant melting curve proposed for the more anisotropic high-T_c superconductors [2]. But if one interprets the magnetization jump in $Bi_2SrCa_2Cu_2O_8$ as evidence for melting, then the melting curve for $Bi_2SrCa_2Cu_2O_8$ apparently approaches T_{c0} *monotonically* at field as low as $\sim 1G$. This behavior is surprising since, at these fields, the vortex separation far exceeds the magnetic screening length. Furthermore, in $YBa_2Cu_3O_{7-\delta}$, the peak effect at $0.35 - 1.5$ T is observed to lie below the resistivity kinks [21] (about $0.8K$ below at 0.5 T). These measurements suggest that, at least for low flux densities, transport measurements may actually not be probing flux lattice melting.

We propose that low-field melting is indeed reentrant. Most low-field experiments which probe magnetization [3,24], thermal properties [6], and transport coefficients [8,24,31,75] actually track T_ℓ, which is progressively more separated from T_m and approaches $T_{XY}(0)$ as the field is reduced. We have already shown that dramatic changes in R_{ab} and R_c occur at T_ℓ. Moreover, the broad peaks in C_V are centered at T_ℓ and they, too, approach $T_{XY}(0)$ as B decreases. Our estimated upper bound for the total entropy release in the temperature range $T_m < T < T_\ell$, as estimated from the $T-$dependence of the internal energy, qualitatively resembles that of Zeldov *et al* (Fig. 6 of [3]) in that it steeply increases as f decreases. At higher fields, the observed (and also calculated) $\triangle S \sim 0.3 - 0.5k_B$ is consistent with the destruction of phase coherence at a *single* transition. By contrast, at low fields, phase rigidity is lost in a two-step process. Most of the entropy release ($\triangle S \geq 0.5k_B$ per vortex per layer) occurs near $T \sim T_\ell > T_m$, whether or not this is a true phase transition. Note that a hysteresis in the resistivity may be observed near T_ℓ due to finite vortex-cutting barriers below T_ℓ. This is not necessarily an evidence for a first-order melting transition at very low fields.

The melting line in the dilute limit may be quite difficult to detect experimentally. Conceivably it may be tracked by the peak effect, by high-resolution IV measurements, or by direct measurement of the shear modulus [44]. Of course, direct observation of a vanishing neutron diffraction pattern as in [4] would be ideal, but this technique is of limited applicability in this density range.

To shed further light on this problem, we have carried out calculations *with mixed boundary conditions*. That is, we allow local density fluctuations in the net z-component of vorticity by using free boundary conditions in $x-$ and $y-$ directions, while retaining periodic boundary conditions along the $z-$axis. Of course, surface effect are now stronger, possibly reducing the melting temperature. Another point is that our uniform-frustration model assumes that $\lambda = \infty$. Therefore, we should proceed with some caution in relating our numerical results to experimental data.

To study the system with these mixed boundary conditions, we again did a simulated annealing run for a single layer of the triangular grid to find the lowest energy configuration. By stacking the resulting state layer by layer, we form the ground state lattice, which, because of incommensurability and the free boundaries, now consists of an imperfect triangular lattice with some defects. This lattice melts at $T/J \leq 1.4$ for the nominal density of $f = 1/24$ on a $26 \times 26 \times 12$ grid. This is slightly below the value $T_m/J \sim 1.5$ found for the fixed density system of 24 layers with periodic boundary conditions. For a nominal density of $f = 1/6$, melting occurs near $T/J \leq 1.15$ with these mixed boundary conditions.

One might think of defining the "magnetization" M_z as the average net vortex density $n \equiv \int n_z(\mathbf{r}) d\mathbf{r}/A$, where $n_z(\mathbf{r})$ is the local vortex density and A is the total area. However, M_z defined in this way suffers from spurious boundary effects, arising from the depletion of vortices near the boundaries in the lattice phase [89]. Upon freezing, the lattice develops a *rigid* free surface of irregular shape, expelling some of the vortices from the rectangular bounding box. The resulting change in density, $\delta n/n$, is an artifact of the open boundary conditions, and we find that it vanishes for large samples as $1/\sqrt{A}$, confirming that it originates from a surface effect.

Instead, we define M_z by a criterion involving the *local Voronoi cell area* $\mathcal{A}_i$, i. e., the area of the generalized Wigner-Seitz cell for vortex i (the shaded area shown in Fig. 22). Before applying the procedure, we first eliminate the thermally induced vortex loops, which are present in addition to the field-induced vortices for $T \geq 0.5 \times T_\ell$. To do this, we pair each antivortex with the nearest vortex in each plane, identifying the resulting pairs as bound dipoles to be excluded from the count (cf. left panel of Fig. 23). Since most such dipole pairs have linear dimensions much

smaller than $1/\sqrt{< n >}$, this criterion is justified. We then perform a Delaunay triangulation on the field induced vortices to determine topological neighbors for each vortex. From the bond configuration thus determined, we obtain its dual, which is the desired Voronoi diagram. A local vortex density at a point $\mathbf{R}$ may then be defined as

$$n(\mathbf{R}) = \sum_i \delta(\mathbf{R} \in \mathcal{A}_i)/\mathcal{A}_i \tag{10}$$

where $\delta(\mathbf{R} \in \mathcal{A}_i) = 1$ if the point $\mathbf{R}$ lies in the Voronoi cell associated with vortex i, and zero otherwise. Next, the local magnetization M_z, which we interpret as the *bulk average density* $< n >$ is calculated from

$$< n >= \sum_{\mathbf{r}_i \in \mathcal{C}} \frac{1}{\mathcal{A}_i}, \tag{11}$$

i. e., as the average of the inverse Voronoi area for vortices lying within a measurement area $\mathcal{C}$ suitably distant from the sample boundary.

In Fig. 24, we show the relative average vortex density (filled circles) along $\hat{z}$, $< n_z > /n_0$, normalized to the nominal density per layer at $f = 1/6$ and $f = 1/24$. For $f = 1/6$, $< n_z >$ shows a sharp jump at T_m to a value about 7 % larger than n_0. For $f = 1/24$, the there is a similar change of about 15 % which is less sharp than at $f = 1/6$ and is centered at T_ℓ. From these two data points, we observe that $[< n > (T_\ell) - n_0]/n_0 \sim f^{-1/2}$. Comparing the result for two different sample areas $L_x L_y$ for $f = 1/24$, we have verified that the observed change is indeed a *bulk* phenomenon, independent of any surface influence. Note that we have about the same number of flux lines($\sim \mathcal{O}(200)$) for both $f = 1/6$ and $f = 1/24$ for our chosen sample sizes of $24 \times 24 \times 12$ and $48 \times 48 \times 12$. While the jump occurs at T_m for $f = 1/6$, we do not observe a similar feature near melting ($T_m = 1.35J$) at $f = 1/24$. Therefore, the cause of the jump in the local vortex density should be sought in the nature of transition at T_ℓ, rather than in the mechanism for flux lattice melting. Note that these jumps resemble those in Fig. 5 of [3] in the "anomalous low-field regime" ($1 < B < 55G$) in the following sense: the fractional change in vortex density decreases, and the jump becomes sharper, as the field increases. Probably, the line density $\langle n_z \rangle$ increases with increasing T for $T_m < T \leq T_\ell$ because the repulsive intervortex interaction is screened by polarizable vortex loops. The 2D analog of this effect is the screening of the repulsion between field-induced vortices by thermally excited vortex-antivortex pairs [90].

Does the jump in flux density occur exactly at the melting transition, or is it more closely connected to the other "transition" at T_ℓ, i. e., to a transition between two liquids with different compressibilities? This question may actually be rather academic, since T_m and T_ℓ may practically merge in real, anisotropic materials at high fields. Eq. (9) gives a rough criterion for T_ℓ in isotropic systems: $1/\ell_c = (c^2 BT/J_z)^{1/\zeta} > p_c$. For anisotropic systems such as $Bi_2SrCa_2Cu_2O_8$ and $YBa_2Cu_3O_{7-\delta}$, a given value of f corresponds to a field which is reduced, relative to the isotropic system, by a factor of J_z/J_{xy}. Therefore, the merging of T_ℓ and T_m, which in isotropic systems occurs around $f \sim 1/18$, should in anisotropic materials occur around f = $(1/18)J_z/J_{xy}$, This anisotropy factor J_z/J_{xy} could be as small as $\mathcal{O}(0.0001)$ in $Bi_2SrCa_2Cu_2O_8$.

VIII. DISCUSSION

A. Analogy to XY Transitions of Slabs of Finite Thickness

In the previous sections, we made following observations from numerical simulations: (i) γ_{zz} vanishes at $T_\ell \neq T_m$ for isotropic system with $f > 1/18$ and $T_\ell(B)$ appears to terminate at T_{XY} for $B \to 0$; (ii) As B changes, it tracks the broad peak in C_V which behaves

$$C_V^{max}(B) \sim -\ln(L_B), \tag{12}$$

and

$$|T_\ell - T_{XY}| \sim L_B^{-2/3}, \tag{13}$$

where $L_B \equiv f^{-1/2} \sim B^{-1/2}$; (iii), T_ℓ, and not T_m, appears to coincide with the principal change in local vortex density which follows

$$\triangle M/B \sim B^{-1/2}. \tag{14}$$

There is a corresponding change in bulk resistances R_{ab} and R_c over the same temperature range; (iv) T_ℓ and T_m seem to merge at a sufficiently high field.

We now summarize some recent experimental observations which appear to be consistent with these numerical results. Schilling et al [7] have reported high resolution calorimetric evidence for a first order transition in $YBa_2Cu_3O_{7-\delta}$, which they interpret as a melting transition. They observe a very sharp delta-function like peak lying on the left shoulder of the broad peak in specific heat in the range of $0.75-9$ tesla, which roughly corresponds to $1/81 < f < 1/6$ in our isotropic sample. The delta-function appears to vanish for densities lower than about 0.5 tesla. This remarkable experiment thus establishes the existence of a first order melting transition line, which empirically follows $|T_m - T_c(0)| \sim L_B^{-1.61}$ over $0.75-9$ tesla. These data are consistent with our numerical results on the following points: (i) a first order melting transition exists, and becomes weaker as the flux density is lowered; (ii) the melting transition is located on the left shoulder of a broader peak in C_V; and (iii) the height of this broad peak and its position generally follow the behavior described in equations 12, 13 and 14. As further evidence of the correspondence, we show in Fig. 25, the data extracted from Fig. 1 of [7] for fields as high as 6 T. At higher fields (> 7 T), the points deviate from the observed power law behavior shown in the Figure.

Another experimental data which agrees well with our numerical results is that of Roulin et al [59]. These workers have reported that both the melting curve $T_m(H)$ and a point they label the "superconducting-normal" (SN) transition as monitored by tracking the maximum in C_V as a function of H both follow the equation $|T - T_c(0)| \sim L_B^{-3/2}$, consistent with our numerical results and the scaling analysis discussed above (to within logarithmic corrections). Welp *et al* [87] have reported a detailed study of ΔM as a function of T and H. The data presented in Fig. 2 of their paper shows that $\triangle M/B \sim B^{-1/2}$ for $1.8 \leq B \leq 5.6$ tesla, once again in agreement with both our numerical results and the scaling data From this data, we conclude that our numerical observations, based on a frustrated 3D XY model, are generally consistent with recent experimental observations.

Most interpretations of these experimental results focused on only one true phase transition in the low field regime, namely a first-order liquid-solid transition. This viewpoint is consistent with our numerical results only if we assume that $T_\ell - T_m$ (where T_ℓ is defined as the temperature where γ_{zz} vanishes) will go to zero in the thermodynamic limit. In the following, we will briefly review a multicritical scaling approach which assumes a single melting transition which happens to be in the vicinity of the zero field XY critical point. Our data are not sufficient to determine without ambiguity whether or not this assumption is correct. Therefore, we follow it by giving an alternative discussion based on the hypothesis that there are actually two separate phase transition lines: $T_m(H)$ for flux lattice melting and $T_\ell(H)$ for complete destruction of any superconducting path (phase coherence) in all directions.

Friesen and Muzikar [91] describe the SN transition at a finite $\mathbf{B}$ in the vicinity of the $f = 0$ XY critical point. Their scaling hypothesis takes the form

$$f_s(B,T) \sim |t|^{2-\alpha}\phi_\pm(B|t|^{-2\nu}) \tag{15}$$

for the singular portion of the free energy density in the XY critical region. Here α and ν are the standard critical exponents describing the specific heat and correlation length of the $f = 0$ critical point, $t = T - T_{XY}(0)$, and $\phi_\pm$ are appropriate scaling functions. B is put in by hand based on the assumption that it is the only relevant length scale. It is plausible, but does not have rigorous justification. Since $\alpha \sim 0$ and $\nu \sim 2/3$ for the $d = 3$ XY model, this expression can be rewritten as

$$f_s(B,T) \sim |t|^2 \ln|t| \phi_\pm(B|t|^{-4/3}). \tag{16}$$

The singular part of $C_V \sim -\partial^2 f_s/\partial t^2$ can now be shown to satisfy the relation (for $T < T_{XY}$)

$$C_V(B,T) \sim \mathcal{C}(x) \ln t \tag{17}$$

where $x = B|t|^{-4/3}$ is the appropriate scaling variable and $\mathcal{C}(x)$ is another scaling function. From this we find (i) that the quantity $C_V/\ln|t|$ has a maximum at some fixed value of x; and (ii) at that fixed value of x, the maximum value $C_v^{max} \sim \ln|t|$. Both (i) and (ii) are in agreement with our numerical data. Similarly, the magnetization is given by $M(B,T) \sim (\partial f/\partial B)_T$. It is readily shown to satisfy

$$M \sim \mathcal{M}(x)(B^{1/2}\ln|x| - \ln B), \tag{18}$$

where $\mathcal{M}$ is another scaling function. A reasonable interpretation of the "jump" ΔM in magnetization is the difference in M between two fixed values x_1 and x_2 of the scaling variable. Then, if the term involving $\ln B$ can be neglected, we have $\Delta M/B \approx B^{-1/2}$ in agreement with our numerical results.

This same scaling picture can be used to interpret the heat of fusion at the first-order melting transition at $T_m(B)$. Assuming that $T_m(B)$ happens to be in the XY critical region, we write the free energy densities below and above $T_m(B)$ as $-t^2\ln|t| f_s(B|t|^{-4/3})$ and $-t^2\ln|t| f_\ell(B|t|^{-4/3})$, where f_s and f_ℓ are two different scaling forms for the free energy density above and below the melting transition. At the melting point, these free energy densities must

be equal. Then a little algebra shows that the jump Δs in the entropy density $S = -(\partial f/\partial T)_B$ takes the form $\Delta s = -t^2 \ln|t|(f_s'(x_m) - f_\ell'(x_m))$, where $x_m = B|t_m|^{-4/3}$ is the value of the scaling parameter at the melting point. Using $B \sim |t|^{4/3}$ along the melting curve, we find that along the melting curve

$$\Delta s \sim B^{3/2} \ln B. \tag{19}$$

Thus the melting transition should have an entropy jump which gets smaller as the field is reduced.

If $T_\ell(B)$ represents a true phase transition as we desribed using the idea of vortex tangles, how can it be understood in terms of the phase coherence? One possibility is a *line of critical points* for a continuous phase transition similar to the XY transition in a semi-infinite slab. This view provides a natural explanation why the scaling theory with the scaling variable $B\xi^2$ should be successful. Mathematically, one can attach a "phantom" cut-line to the core of each vortex segment across which phase slips by 2π. These are benign since continuity and single valuedness of the phase Θ at every point is ensured. However, their shape and motion can be monitored most conveniently to keep track of the spatial and temporal disturbance of the phase coherence which have important consequences such as phase slip dissipation in superconductors. For an isolated vortex segment placed at origin with positive vorticity along $\hat{z}$, the cut-line may lie straight along the positive $\hat{x}$-axis. A negative vortex will then have the cut-line on the negative $\hat{x}$-axis. Once we choose a cut-line for a particular vortex by fixing the reference phase angle, it provides the reference for all other vortices. Note that these cut-lines can only terminate either at the sample boundary or at the core of vortices of opposite charges. When there are several interacting vortices, these cut-lines are no longer straight, and their tortuosity reflects the phase disturbances induced by deformation of the vortex configuration away from perfect lattice. If the vortex lines were straight, we will observe that the cut-lines associated with each segment all line up as we move along a vortex line. Therefore, a cut-line associated with each vortex line will form a semi-infinite cut-sheet, separated from other sheets by roughly $L_B \sim B^{-1/2}$. As the vortex lines become tortuous in the liquid phase above T_m, the cut-sheets will become wrinkled and our system will look like a three dimensional maze walled by these sheets. Both in the vortex solid and line-liquid phases, this maze will allow a arbitrarily curved path connecting both sides(either along $\hat{z}$ or $\hat{x}$-axes) of the sample, and the average width of the path free of the walls will be $\mathcal{O}(L_B)$. We conjecture that it is possible that the phase variables may maintain long range coherence. At low fields(large L_B), this tortuous slab contains many XY phase degrees of freedom which, being confined within the walls, *do not feel* the presence of free vortices, and therefore could conceivably undergo a phase transition in the universality class of a zero-field XY model in a "film" of thickness $\sim L_B$, i. e., a quasi 3D-XY transition. This crosses over to a bulk XY transition as $B \to 0$.

There are two possible objections to this picture. First, our numerical results only hint at, and certainly do not prove, two separate phase transitions. Secondly, the "film" mentioned above is a dynamical rather than an equilibrium film, in the sense that its boundaries are not fixed. It is not clear that such a dynamical object could have an XY phase transition. The boundaries (i. e., cut-sheets of the deformed vortex lines) are, of course, moving subdiffusively [14,92] as long as $\xi_{vz}/d > \mathcal{O}(10)$. This condition, as we confirmed numerically in section VI B, holds true in the range $T_m < T < T_\ell$ and makes the above picture more plausible. It also greatly enhances the chance if we consider pins in real material, since even a single vortex line then becomes collectively pinned into a glassy state.

We now discuss a 3D XY-like transition for the infinite slab of thickness L_B. Such a slab belongs to the G_2-class in Barber's classification of finite size systems [94]). From this identification, we can derive many characteristics of the phase transition. First, consider a thermodynamic quantity for an infinite system in 3D, which varies as $P_\infty(T) \sim C_\infty t^{-\rho}$, where $t = (T - T_c)/T_c$ with T_c the transition temperature for an infinite system and ρ an appropriate critical exponent. For a slab of thickness L_B, a general finite size scaling ansatz dictates that

$$P_{L_B}(T) \sim L_B^\omega Q(L_B^\theta \dot{t}) \tag{20}$$

as $L_B \to \infty, \dot{t} \to 0$ with $\theta = 1/\nu$. The exponent ω is determined by requiring bulk behavior in the limit $L_B \to \infty$; this condition gives $\omega = \rho/\nu$. The transition temperature for a finite $\mathbf{B}$ is shifted

$$(T_c - T_c(L_B))/T_c \sim L_B^{-\lambda} \tag{21}$$

and the shift exponent λ is generally equal to $1/\nu$, as has been discussed for the superfluid transition in bulk ^{4}He of finite thickness by Ambegaokar *et al* [95]. For our purposes, it is sufficiently accurate to take $\nu \sim 2/3$, which then agrees very well with our numerical result(Eq. 13). Eq. 20 needs to be modified for a quantity with a logarithmic divergence; it becomes $P_\infty(T) \sim C_\infty \ln t$ as $t \to 0$, one modifies the ansatz [96] so that we have $P_{L_B}(T) - P_{L_B}(T_0) \sim Q(L_B^\theta \dot{t}) - Q(L_B^\theta \dot{t_0})$, where T_0 is some non-critical temperature. For $\dot{t} \to 0$ at a fixed L_B, we obtain for such a variable

$$P_{L_B}(T_c(L_B)) \sim -C_\infty \theta \ln L_B \tag{22}$$

where we have assumed that $Q(z) = \mathcal{O}(1)$ for $z \to 0$. This prediction is in good agreement with the calculated maximum height of specific heat peak(Eq. 12), which for the 3D XY model, has a weak divergence with $\alpha \sim 0$. Similar results have been discussed for the superfluid transition in He II of finite thickness by Ambegaokar et al [95].

As the field increases, one may eventually reach the limit $L_B/\xi_{XY}(T) < 1$, at which the transition at $T_c(L_B)$ will crossover to a 2D KT universality class and we expect the merging of the two transitions, $T_\ell = T_m$. In our model, we believe this happens for a value of f between 1/6 and 1/18.

IX. OTHER RECENT SIMULATIONS

Towards the completion of this work, we became aware of some of the more recent studies based on similar models. We briefly discuss them in comparison with our main results and interpretations. To avoid confusion, we use our own conventions for the flux density given in terms of the frustration f defined earlier and introduce the anisotropy factor $\Gamma^2 \equiv J_{xy}/J_z$. For an isotropic system, $\Gamma = 1$ while for $YBa_2Cu_3O_{7-\delta}$ it is $\sim \mathcal{O}(10)$ and for $Bi_2Sr_2CaCu_2O_8$, it is $>> \mathcal{O}(100)$. We also use the same notation T_ℓ for the temperature where γ_{zz} drops to zero. Some researchers opted to use T_z.

Nguyen and Sudbø [35] have extended their earlier work on the anisotropic London loop model [34]. Their numerical results in both the vortex structure factor and γ_{zz} for $\Gamma = 1$ with $f = 1/32$ follow a pattern qualitatively similar to our main results for $\Gamma = 1$, $f = 1/24$ [See Figure 6 of [35]] as well as those of Li and Teitel [25,26]. By looking at the dependence of $T_\ell(N_z)$ on the thickness of the system $16 \le N_z \le 96$, and linearly extrapolating the finite size effect, they conclude that $T_\ell^\infty = T_m$ in the thermodynamic limit($N_z \to \infty$). Their argument is based on the following observations:1) T_ℓ decreases with an approximately linear dependence on increasing N_z, $T_\ell(N_z+\delta N_z) \sim T_\ell(N_z) - c\cdot\delta N_z$ with a positive number c. 2) In the thermodynamic limit, below the melting transition($T \sim T_m$), the energy scale for the interlayer phase fluctuation $T^* \sim \xi^2 J_z$ diverges due to long range lattice order. Therefore, the linear progression can not continue below T_m. From these, they conclude that $T_\ell \to T_m$ in the thermodynamic limit.

We agree with the validity of the second assumption on general grounds. However, this does not exclude the possible existence of an intermediate phase in which the interlayer fluctuation may be suppressed due to the quasi-long range phase correlations in a line liquid "phase". With this possibility open, T_m is only a lower bound for the T_ℓ. It should also be noted that γ_{zz} does not show a significant dependence on size in the region where $0.8 < \gamma_{zz} < 1$, in temperatures $T_m < T < 1.8T_m$. It is only at higher temperatures, near where $\gamma_{zz} \to 0$, that the linear dependence of the shift in T_ℓ on N_z is observable. In other words, the size dependence of γ_{zz} is not trivial as temperature varies and one should not expect the same size dependence be uniformly applied over the whole temperature range $T_m < T < T_{XY}$.

Furthermore, the linear dependence of shift in T_ℓ on N_z in the region where $\gamma_{zz} \sim 0$ is anticipated on more general grounds. In the London limit, γ_{zz} measured in the simulation under periodic boundary conditions is

$$\gamma_{zz}(q_x = \pi/\sqrt{N_x N_y}) \sim \frac{J}{V\Gamma^2}\Big[1 - \frac{4J}{N_z\Gamma^2 T\pi} < n_y(q_x = \pi/N_x) n_y(q + x = -\pi/N_x) > \Big] \tag{23}$$

where $n_y(q_x = \pi/N_x)$ is the Fourier component of the vorticity vector field lying along $\hat{y}$ direction. Position of T_ℓ is governed by the condition that the vortex fluctuations make the factor in the bracket vanish. Let us assume that there is a characteristic number of layers N_z^* for which the true thermodynamic transition is realized at T_ℓ^*. For a size N_z smaller than N_z^*, $N_z = N_z^* + \delta N_z (\delta N_z < 0)$, linearization of the condition gives

$$T_\ell(N_z) \sim T_\ell^* + g(T_\ell^*)\delta N_z \tag{24}$$

with $g(T) = \Gamma^2 \partial[< n_y(\pi/N_x) n_y(-\pi/N_x) > /T]/\partial T$. What is the temperature dependence of $< n_y n_y >$? Near T_m, where thermally activated vortex loops *begin* to appear, it is dominated by the vortex loop fugacity factor and is steeply increasing function of T following an S-shaped curve. However, near the foot of γ_{zz}, where our T_ℓ is located, it is numerically observed that it has reached the plateau and the temperature dependence is dominated by the $1/T$ factor. It is also consistent with the interpretation of T_ℓ in terms of XY-type unbinding transition. Since $g(T_\ell) < 0$ and $\delta N_z < 0$ in this region, we then reach the conclusion that $T_\ell(N_z)$ linearly increases away from T_ℓ^* with $c|N_z^* - N_z|$ as N_z decreases from the asymptotic(thermodynamic) limit. Note that we do not assume $T_\ell^* = T_m$ in reaching this conclusion. If one should follow Nguyen and Sudbø and extrapolate the observation of the linear dependence in the limited range of the system size and conclude that $T_\ell^*(B) = T_m(B)$, it also follows that we have a paradoxical consequence of predicting $T_{XY} \to 0$ for the zero field, based on the similar bahavior numerically observed for $\gamma_{\alpha\alpha}$ for $f = 0$.

Following the convention of Koshelev, we employ the *scaled field variable* $h = \Gamma^2 f$ which characterizes the thermodynamics of the mixed state as long as $\lambda \to \infty$. As we pointed out earlier [83], $f = 1/6$ with $\Gamma^2 = 1$ ($h = 1/6$)

represents a situation where the interlayer decoupling sets in right at the melting transition. From our numerical results with h varying from 1/6 to 0, we believe that there is a universal crossover value of scaled density h between 1/6 and 1/18 which separates a *low field* regime from the *high field* regime for which $T_m = T_\ell = T_c(B)$. Koshelev [97] made a numerical observation that $T_\ell \to T_m$. However, it is again made for $\Gamma^2 = J_{xy}/J_z = 36, f = 1/36$, i. e. $h = 1$, equivalent to an extremely dense limit. Recent calculations by Hu and Tachiki [98] based on $f = 1/25, \Gamma^2 = 10$ in a larger system size of $50 \times 50 \times 40$ falls into the same category with $h = 10/25 \gg 1/6$. For this dense limit, they observe that γ_{zz} drops sharply to zero at the melting transition, as we had observed earlier for the $h = 1/6$ case in the stacked triangular XY model [83].

The technical difficulty of simulating the very low field limit ($h < 1/18$) with large number of field induced vortex lines remains largely unsurmounted. To minimize the artificial grid pinning effect, one is required to choose a fairly small value of $f(< 1/32$ for the square grid, $< 1/16$ for the triangular grid). However, choice of a large anisotropy factor to mimic HTSC then tends to push the model into the high field regime as pointed out earlier. To access the truly low field regime($B \ll 1$ tesla for $YBa_2Cu_3O_{7-\delta}$, $\ll 200$ gauss for $Bi_2SrCa_2Cu_2O_8$), we had to employ an isotropic model for a practical value of $f < 1/18$. Summarizing this section, we make educated guess on the thermodynamics of extremely low field limit, where the field-induced vortex degrees of freedom are no longer viable [99]. Here, the transition at T_ℓ takes over the first order melting transition as the *S-N* transition which possibly belongs to the universality class of *zero field transition of XY film* with thickness a_B. The phase for $T_m < T < T_\ell$ may still be considered superconducting in the sense that a superconducting path, however narrow, may exist across a macroscopic distance along $\mathbf{B}$, which defines a tiny, but finite critical current. This may be enhanced by collective pinning of the single lines, but resistance measured with a large driving will show a non-linear IV characteristics and hysteresis as current has to distribute itself among the superconducting paths and normal channels.

The field induced lines in the low field limit, if we take the world-line analogy, are equivalent to extremely massive bosons and eventually drop out of the thermodynamics. They become localized charges which tend to polarize the underlying vacuum and induce a *dielectric breakdown* as the XY medium become more and more polarizable as T increases toward T_ℓ^*. It is somewhat similar to a *metal-insulator* transition in a narrow band-gap semiconductor in which local field gradient(due to the field induced vortices) and shrinking band gap (as $T \to T_\ell$) conspire to a massive generation of screening dipole pairs (vortex loops) leading to a metallic state.

X. CONCLUSIONS

To summarize, we confirmed the existence of a single first order melting transition at high vortex densities. We also showed that upon melting the local vortex density increases due to the screening effect of thermally generated vortex loops. More significantly, however, we observed that, in the absence of disorder, destruction of phase coherence in a superconductor may proceed by two separate transitions at low magnetic fields: a quasi-long range phase coherence parallel to the field disappears at a temperature T_ℓ higher than T_m at which the lattice periodicity disappears and true long range phase coherence is lost. In this low-field regime, the lattice first melts into a liquid of lines with a finite entanglement length along the applied field. These lines eventually disappear through increasing entanglement, and through their interaction with thermally induced vortex and antivortex loops. While the melting transition is best characterized by the disappearance of Bragg peaks for the vortex lines and a delta function peak in the specific heat, there is a narrow region above T_m where we observe dramatic changes in dissipation tensor which coincide with jump in the local vortex density and disappearance of the longitudinal phase rigidity, $\gamma_{zz} = 0$. Instead of being a gradual crossover, we propose that a possible transition at $T_\ell \neq T_m$ sets in at low densities. It tracks the broad peak in specific heat as B increases, obeying the behavior of 3D zero field XY system confined to a semi-infinite slab of finite thickness $L_B \sim B^{-1/2}$. It can alternatively described in terms of appearence of connected vortex tangle which effectively leads to decoupling of neighbouring layers. Within this picture, origins of several puzzling and conflicting anomalies recently obtained on $Bi_2SrCa_2Cu_2O_8$ and $YBa_2Cu_3O_{7-\delta}$ may be understood.

XI. ACKNOWLEDGMENTS

This work has been supported by the Midwest Superconductivity Consortium at Purdue University, through Grant DE-FG02-90ER45427. Calculations were carried out, in part, on the network of SP-2 computers of the Ohio Supercomputer Center.

+ Present address: Schlumberger-Doll Research, Old Quarry Road, Ridgefield, CT 06877.

[1] For an early, comprehensive survey, see A. P. Malozemoff, in *Physical Properties of High Temperature Superconductors-I*, ed. by D. M. Ginsberg (World Scientific, Singapore, 1989), pp. 71-150.
[2] D. R. Nelson, Phys. Rev. Lett. **60**, 1973 (1988).
[3] E. Zeldov, D. Majer, M. Konczykowski, V. B. Geshkenbein, V. M. Vinokur and H. Shtrikman, Nature **375**, 373 (1995).
[4] R. Cubitt, E. M. Forgan, G. Yang, S. L. Lee, D. M. Paul, H. A. Mook, M. Yethiraj, P. H. Kes, T. W. Li, A. A. Menovsky, Z. Tarnawski and K. Mortensen, Nature **365**, 407 (1993).
[5] S. L. Lee, P. Zimmermann, H. Keller, M. Warden, I. M. Savic, R. Schauwecker, D. Zech, R. Cubitt, E. M. Forgan, P. H. Kes, T. W. Li, A. A. Menovsky and Z. Tarnawski, Phys. Rev. Lett. **71**, 3862 (1993).
[6] A. Schilling, R. A. Fisher, N. E. Phillips, U. Welp, D. Dasgupta, W. K. Kwok and G. W. Crabtree, Nature **382**, 6594 (1996).
[7] A. Schilling, R. A. Fisher, N. E. Phillips, U. Welp, W. K. Kwok and G. W. Crabtree, Phys. Rev. Lett. **78**, 4833 (1997).
[8] H. Safar, P. L. Gammel, D. A. Huse, D. J. Bishop, J. P. Rice and D. M. Ginsberg, Phys. Rev. Lett. **69**, 824 (1992).
[9] D. E. Farrell, J. P. Rice and D. M. Ginsberg, Phys. Rev. Lett. **67**, 1165 (1991).
[10] D. E. Farrell, W. K. Kwok, U. Welp, J. Fendrich and G. W. Crabtree, Phys. Rev. **B51**, 9148 (1995).
[11] R. E. Hetzel, A. Sudbøand D. A. Huse, Phys. Rev. Lett. **69**, 518 (1992).
[12] D. Domínguez, N. Grønbeck-Jensen, A. R. Bishop, Phys. Rev. Lett. **75**, 4670 (1995).
[13] R. Šášik and D. Stroud, Phys. Rev. Lett. **75**, 2582 (1995); addendum (to be published).
[14] Seungoh Ryu and D. Stroud, Phys. Rev. **B54**, 1320 (1996); addendum (to be published).
[15] L. D. Landau and E. M. Lifshitz, *Statistical Physics*, 3rd ed., Part 1, (Pergamon, New York, 1980).
[16] Seungoh Ryu, A. Kapitulnik and S. Doniach, Phys. Rev. Lett. **77**, 2300 (1996).
[17] M. J. P. Gingras and D. A. Huse, Phys. Rev. **B53**, 15193 (1996).
[18] M. P. A. Fisher, Phys. Rev. Lett. **62**, 1415 (1989).
[19] Seungoh Ryu, S. Doniach, G. Deutscher and A. Kapitulnik, Phys. Rev. Lett. **68**, 710 (1992).
[20] S. K. Ghosh *et al*, Phys. Rev. Lett. **76**, 4600 (1996).
[21] W. K. Kwok, J. A. Fendrich, C. J. v. d. Beek and G. W. Crabtree, Phys. Rev. Lett. **73**, 2614 (1994).
[22] X. S. Ling *et al*, Phys. Rev. Lett. **76**, 2989 (1996).
[23] X. S. Ling, J. I. Budnick and B. W. Veal, Physica C, **282-287**, 2191 (1997).
[24] D. T. Fuchs, E. Zeldov, D. Majer, R. A. Doyle, T. Tamegai, S. Ooi and M. Konczykowski, Phys. Rev. **B54**, R796 (1996).
[25] Y.-H. Li and S. Teitel, Phys. Rev., **B47**, 359 (1993).
[26] Y.-H. Li and S. Teitel, Phys. Rev. **B49**, 4136 (1994).
[27] T. Chen and S. Teitel, Phys. Rev. Lett. **74**, 2792 (1995).
[28] T. Chen and S. Teitel, cond-mat/9702010, (1997).
[29] H. Safar, P. L. Gammel, D. A. Huse, S. N. Majumdar, L. F. Schneemeyer, D. J. Bishop, D. Lopez, G. Nieva and F. de la Cruz, Phys. Rev. Lett. **72**, 1272 (1994).
[30] D. López, G. Nieva and F. de la Cruz, Phys. Rev. **B50**, 7219 (1994).
[31] C. D. Keener, M. L. Trawick, S. M. Ammirata, S. E. Hebboul and J. C. Garland, Phys. Rev. Lett. **78** 1118 (1997)
[32] C. D. Keener, M. L. Trawick, S. M. Ammirata, S. E. Hebboul and J. C. Garland, Phys. Rev. **B55** R708 (1997).
[33] E. A. Jagla and C. A. Balseiro, Phys. Rev. Lett. **77**, 1588 (1996).
[34] A. K. Nguyen, A. Sudbø and R. E. Hetzel, Phys. Rev. Lett. **72**, 1592 (1996).
[35] A. K. Nguyen and A. Sudbø, *preprint*, (1997).
[36] Z. Tešanović, Phys. Rev. **B51**, 16204 (1995).
[37] D. P. Arovas and F. D. M. Haldane (unpublished).
[38] M. E. Fisher, M. N. Barber and D. Jasnow, Phys. Rev. **A8**, 1111 (1973).
[39] Expressions for these components are given, for example, by W. Y. Shih *et al*, Phys. Rev. **B30**, 134 (1984).
[40] See, for example, J. S. Chung, K. H. Lee, and D. Stroud, Phys. Rev. **B40**, 6570 (1989).
[41] Chapter 16, page 710 of *Numerical Recipes in C* by W. H. Press, S. A. Teukolsky, W. T. Vetterling and B. P. Flannery, Cambridge Univeristy Press, (1992).
[42] See, for example, K. H. Lee, D. Stroud, and S. M. Girvin, Phys. Rev. **B48**, 1233 (1993).
[43] C. J. Lobb (calculation of depinning energy for pancakes in triangular and square lattices).
[44] H. Pastoriza and P. H. Kes, Phys. Rev. Lett. **75**, 3525 (1995)
[45] D. R. Nelson, in *Correlations and transport in vortex liquids*, edited by K. Bedell, M. Inui, D. Meltzer, J. R. Schrieffer and S. Doniach, (Addison-Wesley, New York, 1991) .
[46] A. P. Gottlob and M. Hasenbusch, Physica **A201**, 593 (1993).
[47] D. R. Nelson and J. Toner, Phys. Rev. **B24**, 363 (1981).
[48] L. Onsager, Nuovo Cimento Suppl. **6**, 249 (1949).
[49] R. P. Feynman, in *Progress in Low Temperature Physics*, vol.I, edited by C. J. Gorter (North-Holland, Amsterdam, 1955).
[50] G. Khoring, R. E. Shrock and P. Wills, Phys. Rev. Lett. **57**, 1358 (1986); G. Khoring and R. E. Shrock, Nucl. Phys. B **288**, 397 (1987).
[51] S. R. Shenoy, Phys. Rev. **B42**, 8595 (1990).

[52] G. Williams, Phys. Rev. Lett. **59**, 1926 (1987); G. Williams, Phys. Rev. Lett. **68**, 2054 (1992); G. Williams, Phys. Rev. Lett. **71**, 392 (1993).
[53] H. Kleinert, *Gauge Fields in Condensed Matter*, vol I, pp. 541 (World Scientific, Singapore, 1989).
[54] See Chapter 9 of P. M. Chaikin and T. C. Rubensky, *Principles of Condensed Matter Physics*, (Cambridge University Press, 1995).
[55] G. Williams, J. Low Temp. Phys. **101**, 421 (1995).
[56] J. H. Akao, Phys. Rev. **E53**, 6048 (1996).
[57] N. K. Kultanov and Y. E. Lozovik, Phys. Lett. **A198**, 65 (1995).
[58] See data presented in M. A. Howson, I. D. Lawrie and N. Overend, Phys. Rev. Lett. **74**, 1888 (1995); N. Overend, M. A. Howson and I. D. Lawrie, Phys. Rev. Lett. **72**, 3238 (1994).
[59] M. Roulin, A. Junod and E. Walker, Science **273**, 1210 (1996).
[60] Any quantity γ which obeys a differential equation of the form $d\gamma/dt = -\exp(-C\gamma)$, where t denotes Monte Carlo "time" and C is a positive constant, has such a time dependence as an analytical solution. Such an equation might be expected to describe γ if its time-dependence were activated, with an activation energy $\Delta E \propto 1/\gamma$. In this scenario, the time dependence of γ would become slower as γ itself shrank, leading to the logarithmic dependence seen. This logarithmic relaxation behavior is reminiscent of the reptation relaxation model of dangling chains inside polymer melts [cf. chapter 8 of P.-G. de Gennes, *Scaling Concepts in Polymer Physics* (Cornell University Press, Ithaca, 1979)]. Indeed, for $T_m < T < T_\ell$, vortex lines in our model are expected to have a significant barrier for cutting and may be viewed as a system of directed polymers but with long range interactions. For $T > T_\ell$, polymer analogy completely breaks down because of the dominance of unbound vortex loops(analogous to polymer-antipolymers!) .
[61] P. Kim, Z. Yao and C. M. Lieber, Phys. Rev. Lett. **77**, 5118 (1996).
[62] G. Carneiro, Phys. Rev. **B45**, 2391 (1992); **B45**, 2403 (1992).
[63] B. Chattophadyay and S. R. Shenoy, Phys. Rev. Lett. **72**, 400 (1994).
[64] J. S. Langer and M. E. Fisher, Phys. Rev. Lett. **19**, 560 (1967); J. S. Langer and V. Ambegaokar, Phys. Rev. **164**, 498 (1967).
[65] M. C. Hellerqvist, S. Ryu, L. W. Lombardo and A. Kapitulnik, Physica **C230**, 170 (1994).
[66] See Chapter 7 of Seungoh Ryu, Ph. D. Thesis (Stanford University, 1995) (unpublished).
[67] M. Kardar and Y.-C. Zhang, Phys. Rev. Lett. **58**, 2087 (1987).
[68] L. Balents and M. Kardar, Phys. Rev. **B49**, 13030 (1994).
[69] See Tables 2 and 3 compiled by J. Krug and H. Spohn in *Solids Far From Equilibrium: Growth, Morphology and Defects* edited by C. Godréche (Cambridge University Press, NY, 1990).
[70] L. Civale, A. D. Marwick, T. K. Worthington, M. A. Kirk, J. R. Thompson, L. Krusin-Elbaum, Y. Sun, J. R. Clem and F. Holtzberg, Phys. Rev. Lett. **67**, 648 (1991).
[71] C. A. Murray, P. L. Gammel, D. J. Bishop, D. M. Mitzi and A. Kapitulnik, Phys. Rev. Lett. **64**, 2312 (1990).
[72] Z. Yao, S. Yoon, H. Dai, S. Fan and C. M. Lieber, Nature **371**, 777 (1994).
[73] C. H. Recchia, C. H. Pennington, H. Hauglin and G. P. Lafyatis, Phys. Rev. **B52**, 9746 (1995).
[74] S. Dapore-Schwartz, N. G. Woodard and G. P. Lafyatis, Phys. Rev. **B55**,m 5655 (1997).
[75] W. K. Kwok, S. Fleshler, U. Welp, V. M. Vinokur, J. Downey, G. W. Crabtree and M. M. Miller, Phys. Rev. Lett. **69**, 3370 (1992).
[76] For example, see Fig. 1 of [75]. The jump is most pronounced for $1.5 < B < 4$ tesla.
[77] J.-P. Bouchaud, M. Mezard and J. S. Yedidia, Phys. Rev. **B46**, 14686 (1992).
[78] T. Giamarchi and P. L. Doussal, Phys. Rev. **B52**, 1242 (1995).
[79] G. D'Anna, P. L. Gammel, H. Safar, G. B. Alers, D. J. Bishop, J. Giapintzakis and D. M. Ginsberg, Phys. Rev. Lett. **75**, 3521 (1995).
[80] A. E. Koshelev and V. M. Vinokur, Phys. Rev. Lett. **73**, 3580 (1994).
[81] M. C. Hellerqvist, D. Ephron, W. R. White, M. R. Beasley and A. Kapitulnik, Phys. Rev. Lett. **76**, 4022 (1996).
[82] N. Grønbech-Jensen, A. R. Bishop and D. Domínguez, Phys. Rev. Lett. **76**, 2985 (1996).
[83] Seungoh Ryu, Monica Hellerqvist, S. Doniach, A. Kapitulnik and D. Stroud, Phys. Rev. Lett. **77**, 5114 (1996).
[84] G. Briceno, M. F. Crommie and A. Zettl, Phys. Rev. Lett. **66**, 2164 (1991).
[85] K. E. Gray and D. H. Kim, Phys. Rev. Lett. **70**, 1693 (1993).
[86] R. Liang, D. A. Bonn and W. N. Hardy, Phys. Rev. Lett. **76**, 835 (1996).
[87] U. Welp, J. A. Fendrich, W. K. Kwok, G. W. Crabtree and B. W. Veal, Phys. Rev. Lett. **76**, 4809 (1996).
[88] In both [13] and [14], the contribution to the total internal energy coming from the temperature dependence of the coupling strengths of the effective free energy functional has been neglected. leading to an underestimate of the value for the heat of melting. When this temperature dependence is taken into account, the results of [14] give $\triangle S \sim 0.28 k_B$. Updated LLL results also have a similar value.
[89] C. Ebner and D. Stroud, Physica **C162-64**, 1469 (1989).
[90] S. Doniach and B. A. Huberman, Phys. Rev. Lett. **42**, 1169 (1979).
[91] M. Friesen and P. Muzikar, preprint ; Katerina Moloni *et al*, Phys. Rev. Lett. **78**, 3173 (1997).
[92] A. T. Dorsey, Phys. Rev. **B46**, 8376 (1992).

[93] L. I. Glazman and A. E. Koshelev, Physica **C173**, 180 (1991).
[94] M. N. Barber, in *Finite-size scaling*, edited by C. Domb and J. L. Lebowitz, (Academic Press, 1983) .
[95] V. Ambegaokar, B. I. Halperin, D. R. Nelson and E. D. Siggia, Phys. Rev. **B21**, 1806 (1980).
[96] M. E. Fisher, in *Critical Phenomena*, edited by M. S. Green, (Academic Press, New York, 1971) .
[97] A. E. Koshelev, *preprint*, (1997).
[98] Xiao Hu, Seiji Miyashita and Masashi Tachiki, *preprint*, (1997).
[99] For a hypothetical isotropic superconductor with $d \sim \xi \sim 100\mathring{A}$, $\mathrm{L}_x \times \mathrm{L}_y \times \mathrm{L}_z \sim 0.1 \times 0.1 \times 10^{-3}\mathrm{cm}^3$, we have about $\mathcal{N}_\phi \sim 10^{13}$ "grains" of the XY model. For a given field B(in gauss), the number of pancake vortex degrees of freedom is $\mathcal{N}_v^{2D} \sim 10^{-5}B/(10^{-6}\phi_0) \sim \mathcal{O}(10^8) \times B$. This number will begin to match that of XY degrees of freedom if $B \sim$ 10tesla. Note that if the lattice melts into a line liquid with an infinite correlation length along $\hat{z}$, the relevant degrees of freedom right at T_m will be $\mathcal{N}_v^{3D} \sim 10^{-2}B/\phi_0 \sim 10^5 B$. For the speculative picture of T_ℓ as the XY transition of a thick film, a crossover from the "finite slab" to the 2D XY regime should occur when $a_B \sim \mathcal{O}(\xi)$. This is met when $B \sim$ 10tesla. For this hypothetical sample, one may predict that for $B >$ 10tesla, the SN transition is dominated by the vortex degrees of freedom and a separate transition at T_ℓ is pre-empted by the first order melting transition, since the lattice melts into a 2D-slab regime directly. On the other hand, as B decreases below 10 tesla toward zero, the melting transition should follow a finite size scaling behavior as the vortex "line" degrees of freedom falls below that of thermodynamic limit, while the XY degrees of freedom takes charge and drive the transition at T_ℓ of the thick, but tortuous XY slab of finite thickness $\sim a_B$.

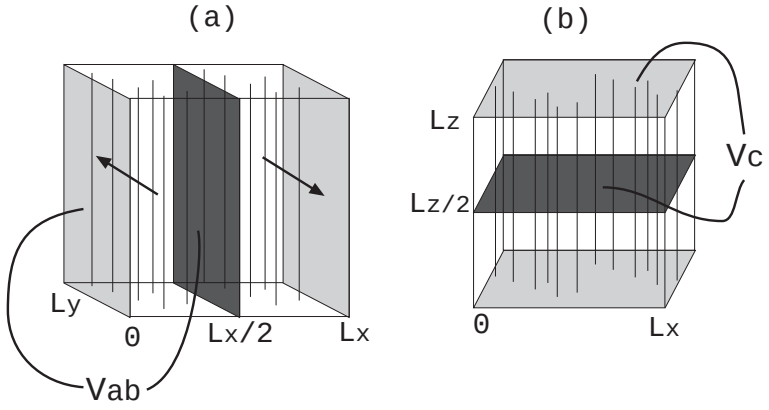

FIG. 1. Geometry for the dynamic calculations described in the text. (a) To probe the shear modulus, current is injected uniformly into plane Σ_{in} and extracted uniformly from Σ_{out}. The arrows indicate directions of the Lorentz forces acting on the lines in the two half volumes (in opposite directions, because of the periodic boundary conditions). (b) To probe the c-axis resistance, the currents are injected and extracted uniformly from the two planes indicated; the voltage drop between the planes is measured as in (a).

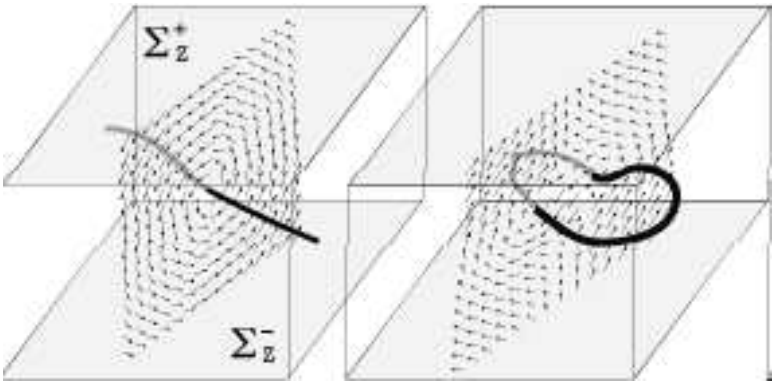

FIG. 2. Two illustrative phase configurations, one with net vorticity piercing the sample parallel to the xy-plane (left panel), and one with zero net vorticity but containing a bound vortex loop (right panel).

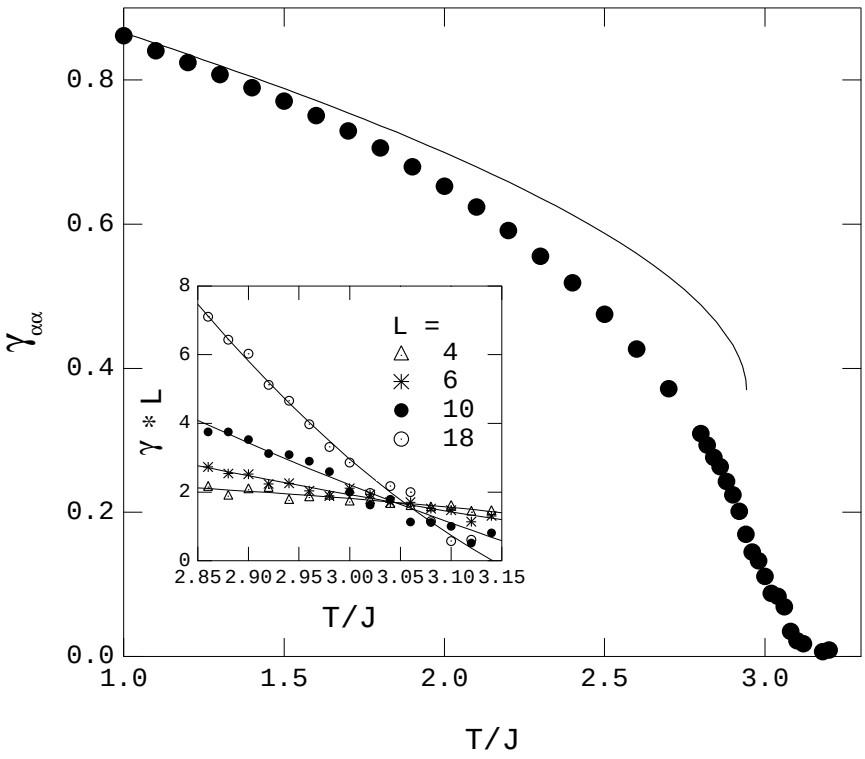

FIG. 3. γ_{zz} from Monte Carlo with 10,000 ($T/J < 2.7$) to 50,000 ($T/ \geq 2.7$) MC sweeps. The line represents a calculation based on the harmonic self-consistent approximation. The inset shows the finite size scaling analysis to locate $T_{XY} = 3.04 \pm 0.02J$.

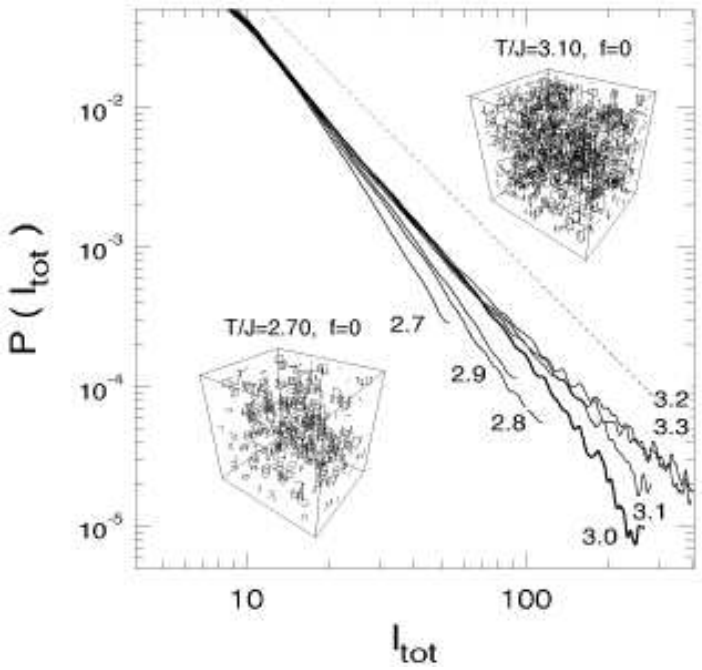

FIG. 4. Size distribution of *connected* vortex segments for $f = 0$. The insets show typical vortex configurations for $T/J = 2.7$ and 3.1.

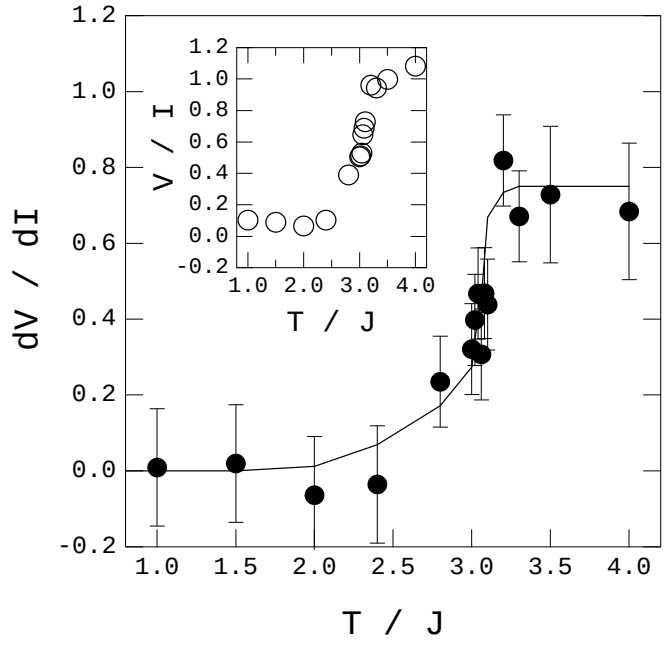

FIG. 5. Dissipation ($dV/dI = [V(I = 0.083) - V(I = 0.043)]/0.04$) across the XY transition, $T_{XY} = 3.04J$. A uniform current of I/I_c per grain is flown through yz planes. The inset shows $\rho \equiv V/I$ at $I = 0.083I_c$.

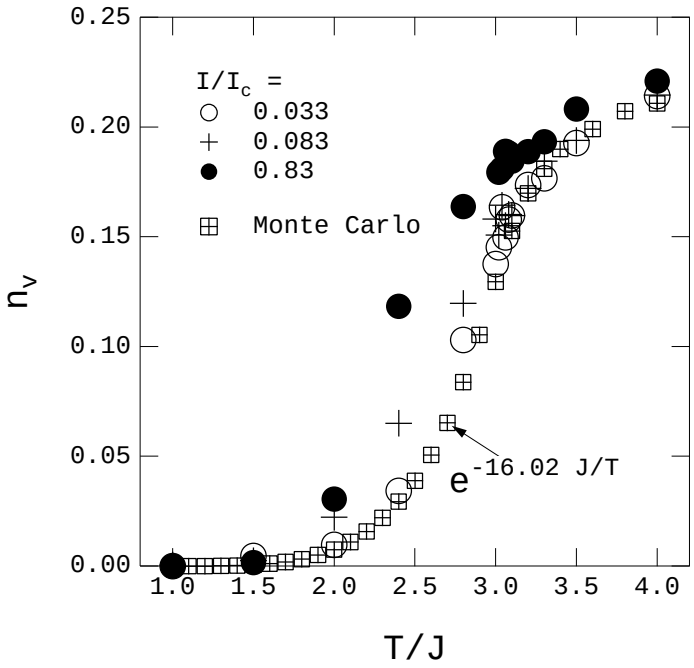

FIG. 6. Average number of vortex segments in equilibrium(Monte Carlo) and with various bias current densities(RSJJ dynamics). The equilibrium density very closely follows an activated form with $U = 16J$ for $T < T_{XY}$.

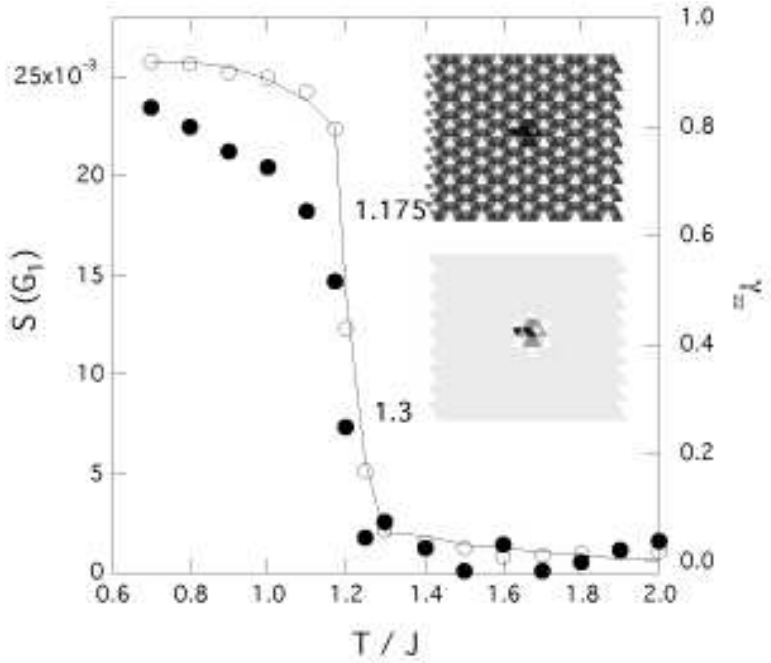

FIG. 7. Normalized Bragg intensity(open circles) and γ_{zz}(filled circles) for $f = 1/6$. The solid line is guide for the eyes. The insets show the real space density correlation $< n_z(r,z)n_z(0,0) >$ for the local z-vorticity taken over 40,000 MC sweeps.

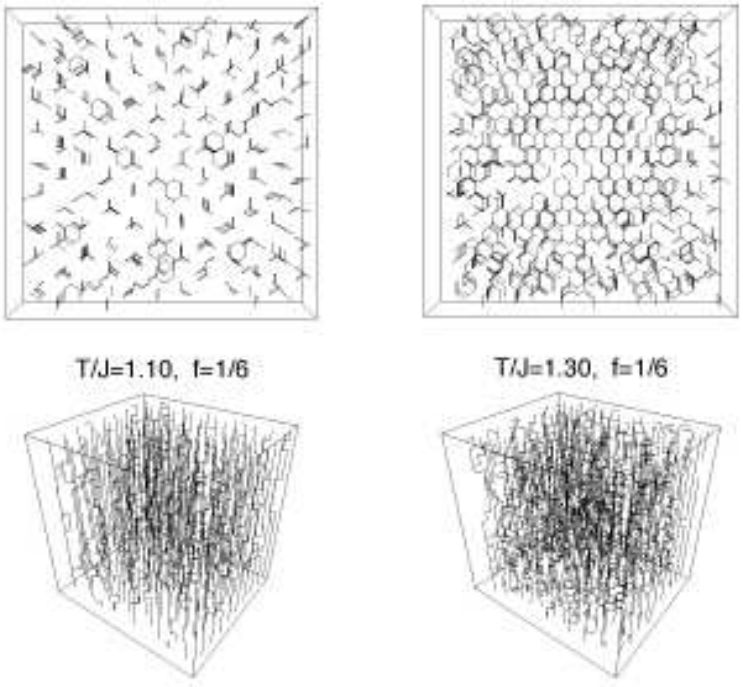

FIG. 8. Typical flux line configurations at for two temperatures ($T/J = 1.1$ and 1.3) spanning the melting temperature at $f = 1/6$, plotted for an $18 \times 18 \times 18$ grid. The upper panels are top views.

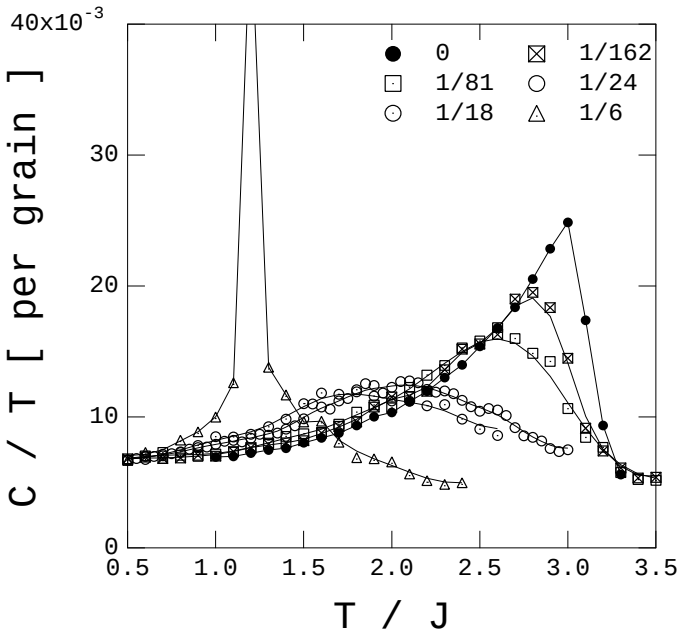

FIG. 9. Specific heat per grain for various frustrations. For $f = 1/6$, C_v at $T = 1.2$ shows a clear divergent behavior, apart from other dilute cases.

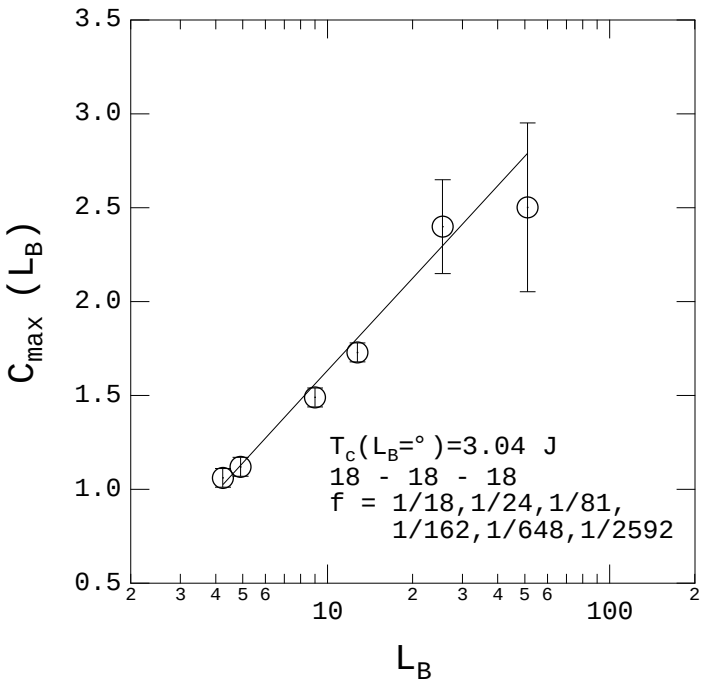

FIG. 10. Dependence of peak height of C_v on the magnetic length L_B. The line is guide for the eyes.

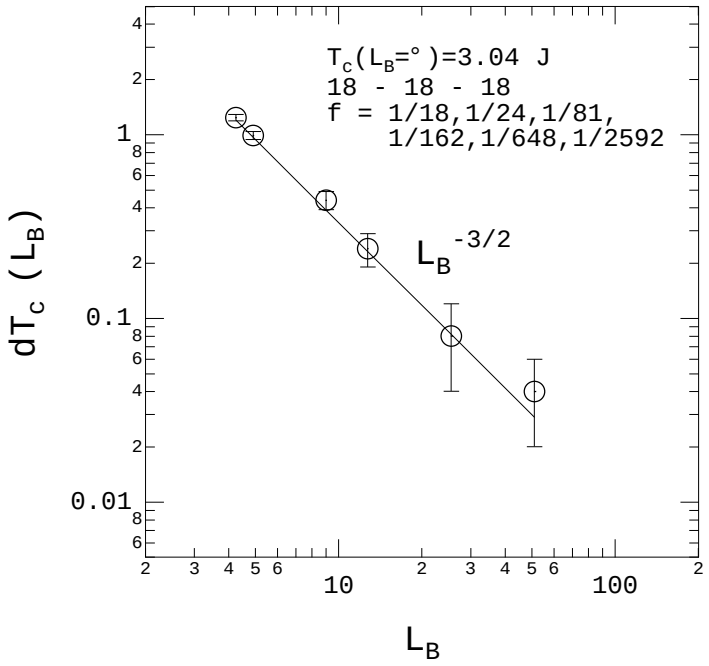

FIG. 11. Shift of peak in C_v from the $f = 0$ position(T_{xy}^0) vs. the magnetic length L_B. The line($\sim L_B^{-3/2}$) is guide for the eyes.

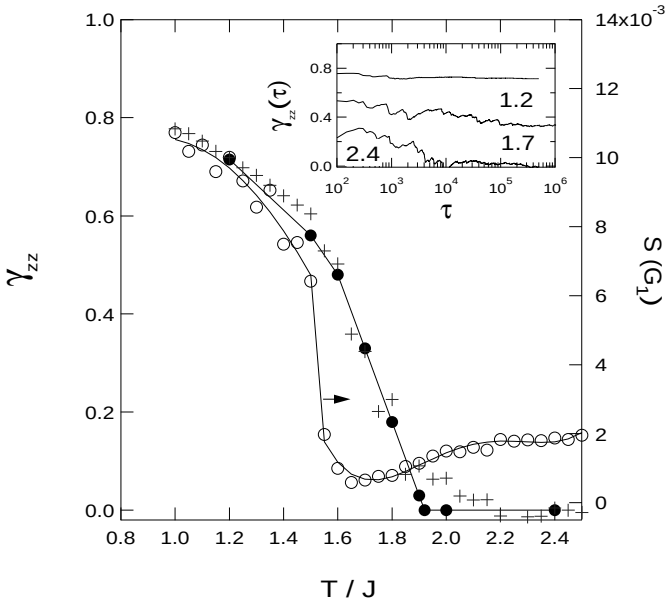

FIG. 12. Normalized Bragg intensity (open circles; 5×10^4 MC sweeps) and γ_{zz} (filled circles: $5 \times 10^5 - 10^6$ MC sweeps; crosses: 5×10^4 MC sweeps) for $f = 1/24$. The solid lines are guides for the eyes. The inset shows the dependence of $< \gamma_{zz} >$ on the accumulation time, as discussed in the text.

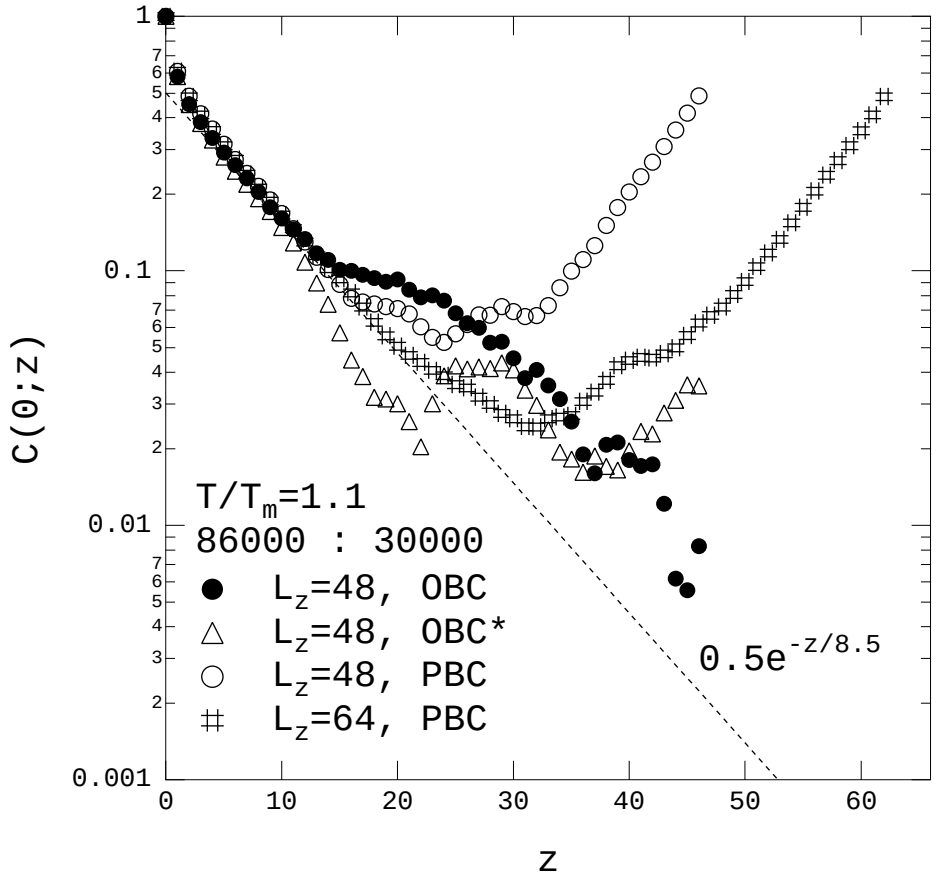

FIG. 13. Phase correlation function $c(\mathbf{0}; z)$ for various system sizes and boundary conditions.

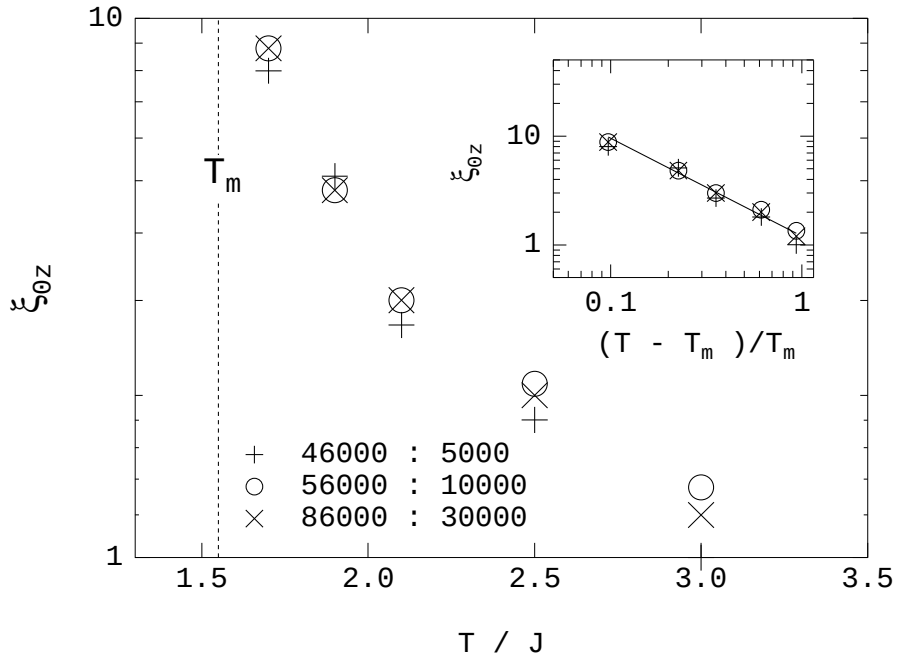

FIG. 14. Longitudinal phase correlation length ξ_{z0} determined from fitting $c(\mathbf{0}; z)$ to the form $a \exp[-z/xi_{z0}]$ for $z < \xi_x(T)$ as discussed in the text.

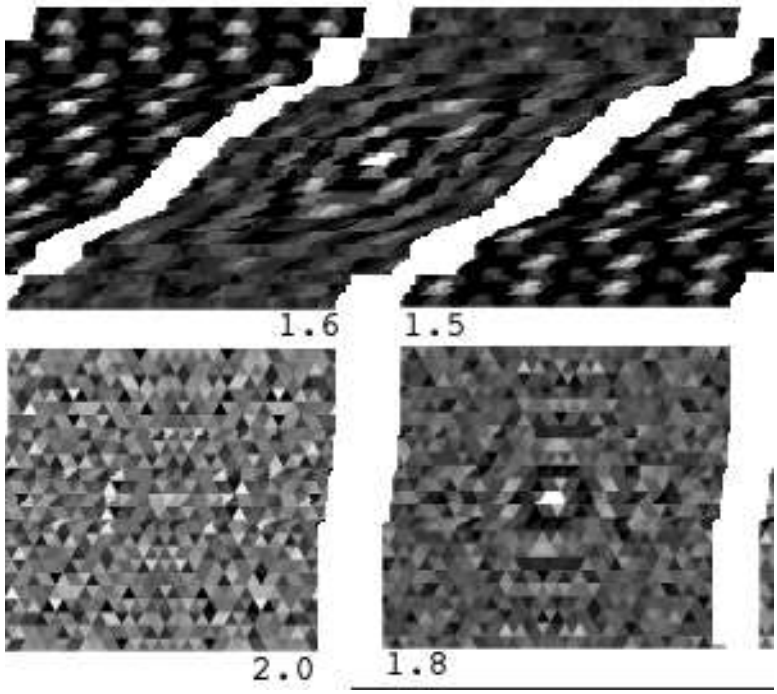

FIG. 15. Real space top-to-bottom density correlation function $< n_z(r, z = 12)n_z(0, 0) >$ for $T/J = 1.5, 1.6, 1.8$ and 2.0 for $f = 1/24$ in a $24 \times 24 \times 24$ grid. Melting occurs around $T_m/J = 1.55$ while line-like correlations (white spot at the center) vanish around $T/J = 2.0 \sim T_\ell/J$. 50,000 MC steps for each temperature.

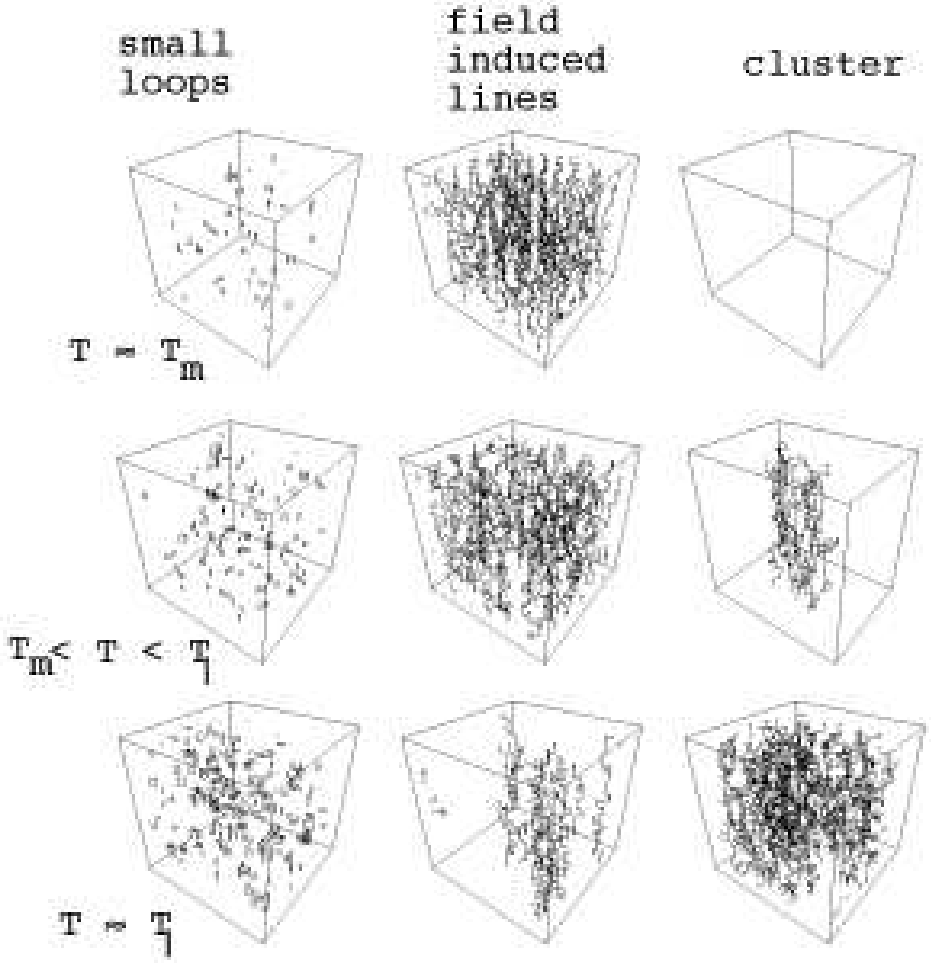

FIG. 16. Vortex configurations for temperatures T in the range $T_m \leq T \leq T_\ell$. The left column shows the portion of vortex fluctuations which form bound loops. The center column shows mainly those field-induced vortex lines which are not entangled, while the right column shows the largest cluster of entangled lines (as defined in the text).

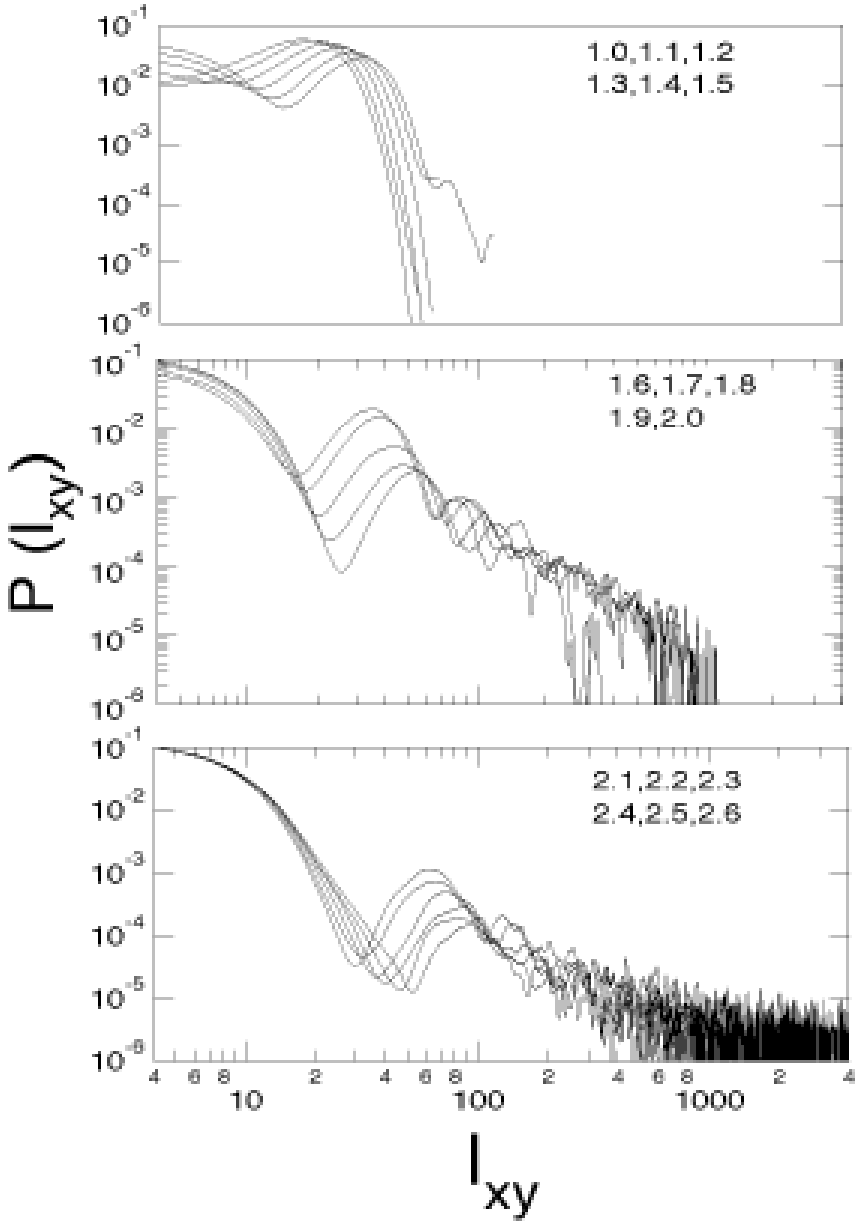

FIG. 17. The distribution of transverse vortex lengths ℓ_{xy} projected onto the xy-plane ℓ_{xy} for three sets of temperatures in the (a) lattice, (b) line liquid, and (c) tangled vortex web states.

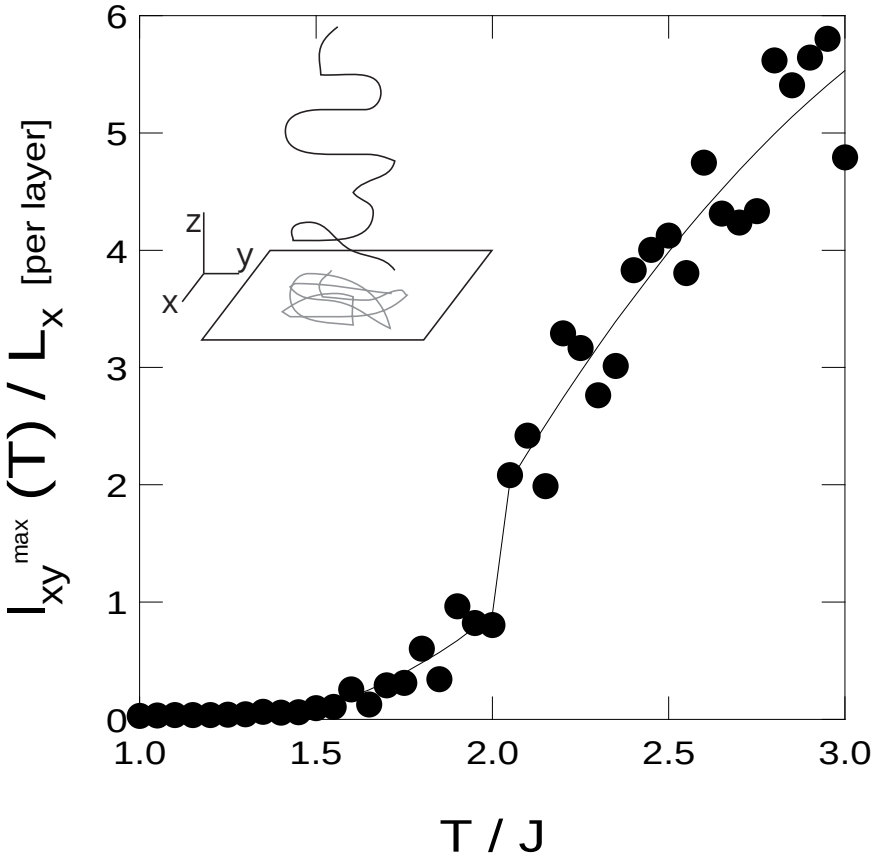

FIG. 18. Maximum projected lateral vortex length ℓ_{xy}, given in terms of the lateral box dimension (=48), and normalized per layer in a $24 \times 24 \times 24$ grid with $f = 1/24$.

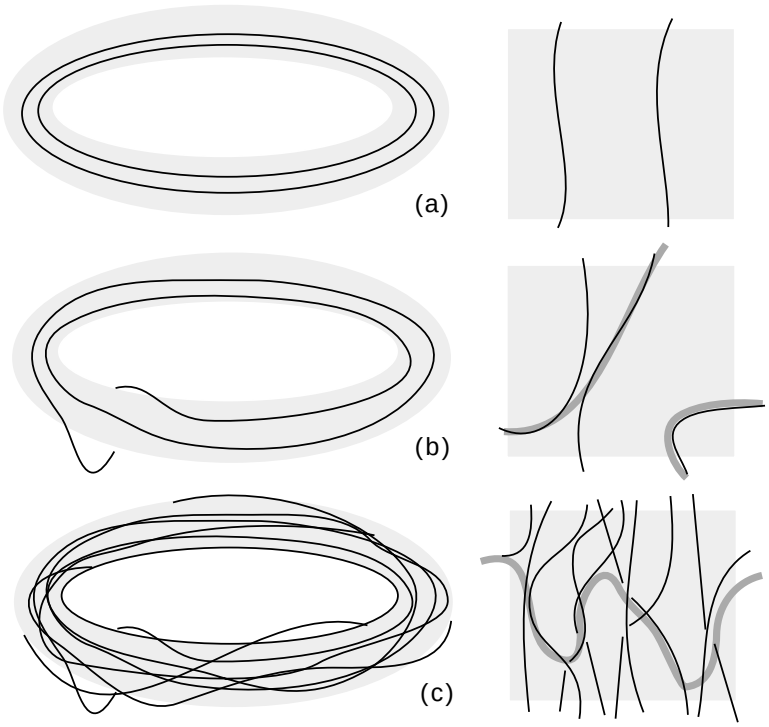

FIG. 19. Effect of switching connections among entangled flux lines in a torus geometry [panel (a)] and in an infinite plane with open boundary conditions. For the case of only two lines [(b)], note that it is necessary to make a long excursion spanning the whole plane to change the global winding number. The latter may be easily induced in a dense environment through collective occurrence of local reconnections [panel (c)].

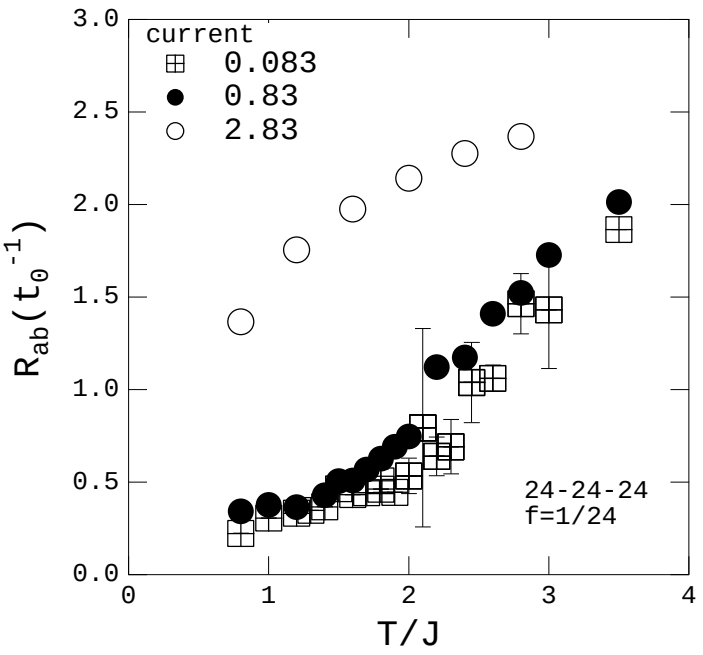

FIG. 20. Calculated bulk in-plane resistance vs. T for $f = 1/24$. Currents of $0.083 - 2.83 I_c$ per grain were injected uniformly into an yz plane.

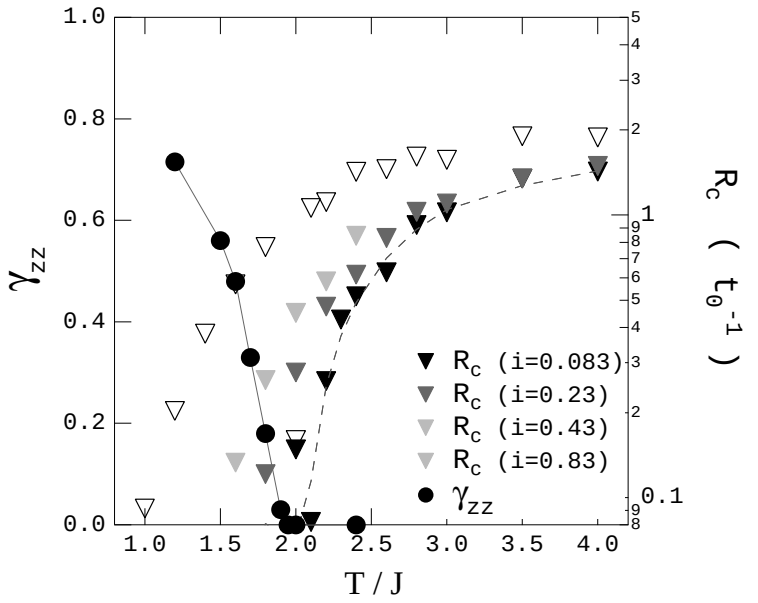

FIG. 21. Calculated $c-$axis resistance (arbitrary units) vs. T for $f = 1/24$. A current of $0.083\mathrm{I}_c$ per grain is injected uniformly into a plane. The inset shows the same results, but with temperature rescaled to model a hypothetical *isotropic* high-T_c superconductor as in the previous Figure.

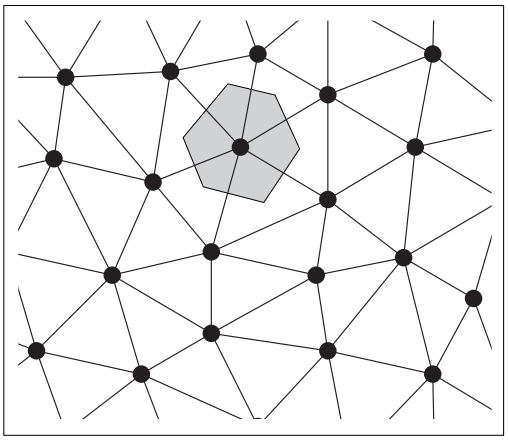

FIG. 22. Example of the local Voronoi cell occupied by a vortex.

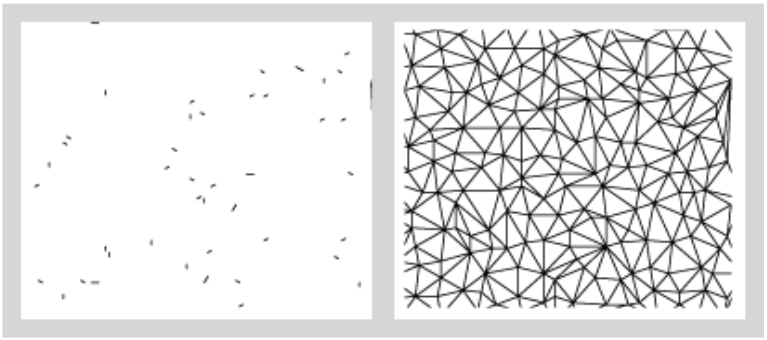

FIG. 23. Example of the vortex configuration in a xy-plane at $z = 6$ in a 48-48-12 system with $f = 1/24$ at T_ℓ. The black dots are field induced vortices, gray dots connected by lines are bound dipoles identified. The right panel shows the Delaunay triangulation applied to the field induced vortices only.

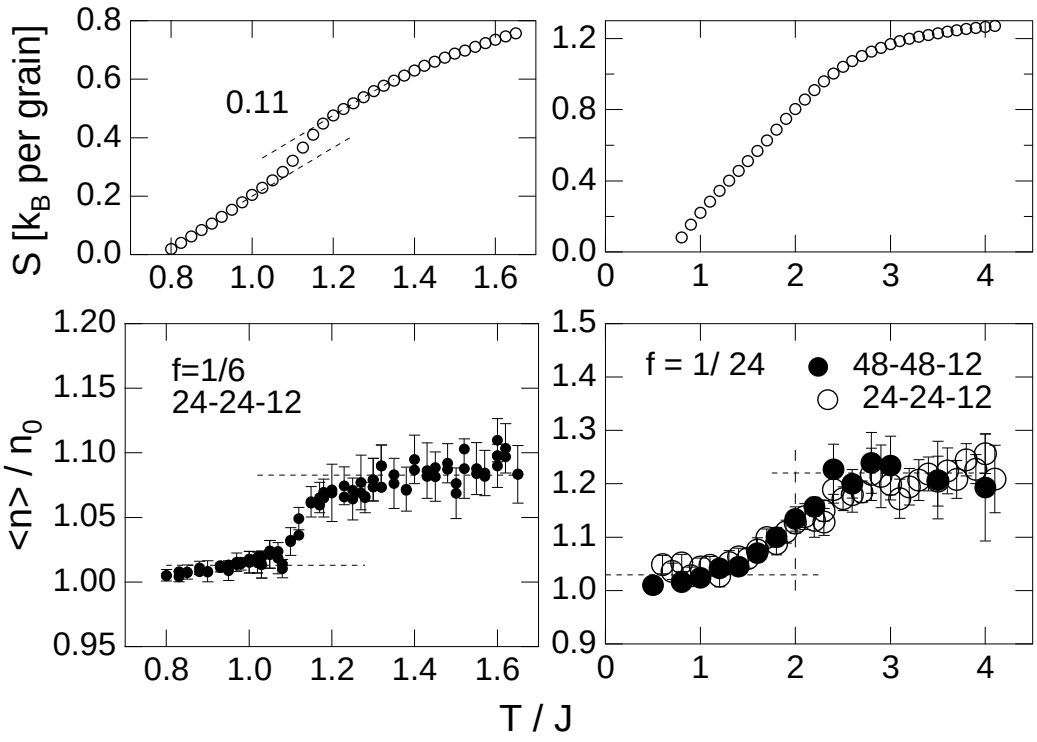

FIG. 24. Entropy S (upper panel) and normalized vortex density (lower panel) for $f = 1/24$ and $1/6$ in $24 \times 24 \times 12$ and $48 \times 48 \times 12$ systems with open boundary conditions. The error bars denote the rms deviations from layer to layer.

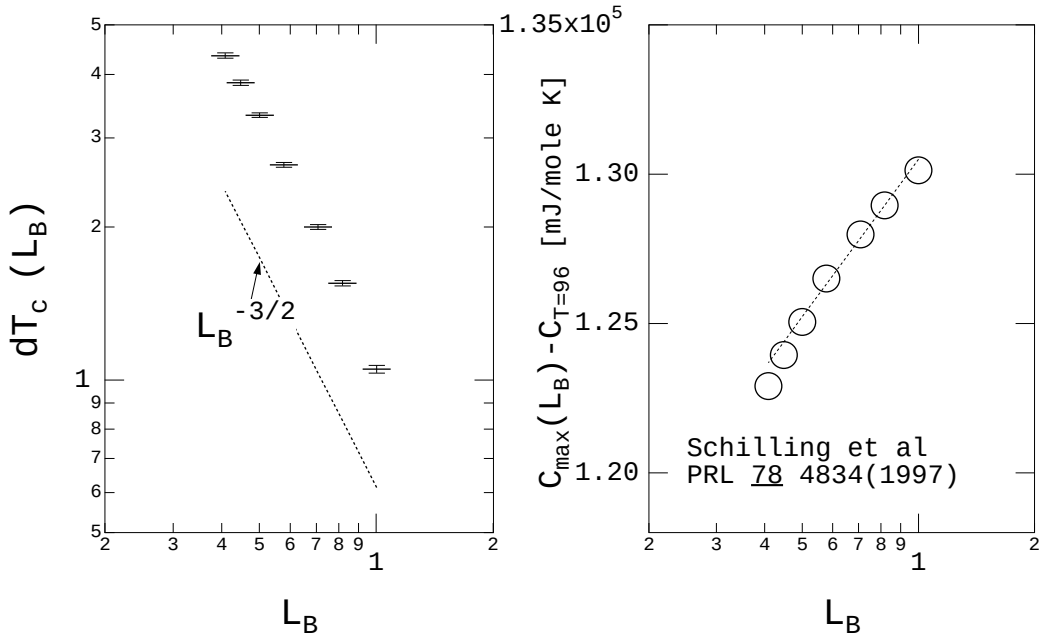

FIG. 25. Dependence of "broad" peak maximum in specific heat and their shift in temperature on the magnetic length L_B taken from Schilling et al [7].